Chapter 7

Paleoplacer Uranium Mineralization Potential in Keonjhar QPCs: Mineralogy, Source Terrain and Geochemical Proxies

7.1. Introduction

Uranium resources are mainly located in Australia (31%), followed by Kazakhastan (12%), Canada (9%), South Africa (6%), United States (4%) and India (2%) (Red Book 2010). In India, known deposits for future production are identified within few provinces such as: uranium province of Cuddapah Basin of Andhra Pradesh, uranium province of Mahadek Basin of Meghalaya, uranium provinces of Bhima and Kaladgi Basins of Karnataka, uranium province of North Delhi Fold belt of Rajasthan and Singhbhum uranium province of Jharkhand and Odisha (Awati and Grover 2005; Chaki 2010; Red book 2010; Chaki et al. 2010; Vasudeva Rao et al. 1989). According to the IAEA (2013) uranium mineralization in sedimentary rocks are commonly classified into nine major genetic types such as the *quartz-pebble conglomerate type mineralization (QPC type), unconformity-related uranium mineralization, surficial uranium mineralization, sandstone-hosted uranium mineralization, collapse breccia pipe hosted uranium mineralization, coal-lignite hosted uranium mineralization, carbonate-uranium mineralization, phosphorite-uranium mineralization, and black shale-hosted uranium mineralization* (Mahadevan 1988; Dahlkamp 1989; Cuney 2010; 2014). Uranium mineralization in the Singhbhum Uranium Province of Jharkhand and Odisha includes two distinct types of genetic mineralization- (a) sediment-hosted Quartz Pebble Conglomerate (QPC) detrital uraninite-bearing

reduced *paleoplacer* type and (ii) metamorphic rock hosted shear-controlled *hydrothermal* type. Previous workers already documented uraniferous QPCs from early Archean to late Proterozoic supra-crustals of the Dhanjori Group and its equivalent along northern periphery and Mahagiri-Keonjhar- Mankaharchua siliciclastics in the southern periphery of the Singhbhum craton (Fig. 7.1) (Mahadevan 1988; Viswanath and Mahadevan 1988; Vasudeva Rao et al. 1988; Viswanath et al. 1988; Mishra et al. 2008; Chakarabarti et al. 2013; Mukhopadhyay et al. 2014). Mukhopadhyay et al. (2016) documented uraniferous QPCs of the Mahagiri Quartzite and detrital uraninite has been described from drill core samples.

Preliminary radioactivity survey by Atomic mineral directorate (AMD) suggests the presence of radioactivity in basal conglomeratic (QPC) associations in some areas of the presently studied Keonjhar Quartzite. Drill cores are not yet available from the from the study area. It is obvious that in surface samples within supergene weathering profile, chance of survival of uraninite is very slim. However, I have studied the surface QPC samples from the Keonjhar Quartzite from geochemical and mineralogical aspects to assess the possible proxy indicators of uranium-thorium mineralization in absence of drill core samples. The study could indicate any potential detrital uraninite-bearing reduced paleoplacer beneath the supergene carapace as recorded from the Mahagiri Ranges from the southern margin of the Singhbhum craton (Mukhopadhyay et al. 2016).

Further, the composition of sedimentary rocks makes important contributions in interpreting tectonics of the source terrain because records of ancient crusts at the sediment source are mostly partially preserved or may be completely destroyed after the accumulation sediments (Taylor and McLennan 2009). To understand the nature

of the upper continental crust during Archean time the sediments sourced from such old crustal blocks are to provide major inputs (*e.g.*, Dickinson and Suczek 1979; Dickinson et al. 1983; Dickinson 1985; Taylor and McLennan 1985, 2009; Veizer and Mackenzie 2003, 2005). The potential of Paleo-Mesoarchean continental crust as the source of the urnaiferous QPCs bears important implications for the development of uraninite plaeoplacer deposits. The main identification property for the tectonic setting of the sedimentary basin comes from the compositional variation of the different components (Nesbitt and Young 1982,1984; Bhatia 1983, 1985; Bhatia and Crook 1986; Roser and Korsch 1986, 1988; McLennan and Taylor 1991; Condie 1993; Johnsson and Basu 1993; McLennan et al. 1993; Fedo et al. 1995; Nesbitt et al. 1997; Cullers and Podkovyrov 2000, 2002; Bhatt and Ghosh 2001; Nesbitt 2003; Zimmermann and Bahlburg 2003, 2010; Armstrong-Altrin et al. 2004). Ghosh et al. (2016) suggested passive margin setting and the presence of both mafic and felsic components in the source terrain of the Keonjhar Quartzite from mainly the chemical compositions of the arenite. I explore here further the compositions of the QPCs and host sandstones for understanding the tectonic setting of the source terrain with regard to the potential of U-Th minerals as source of detrital radioactive paleoplacer.

The radioactive Quartz Pebble Conglomerates (QPC) in the Keonjhar Quartzite occur in the basal part of the succession. Radioactivity is recorded in two pebbly conglomerates in the basal part of the Asurkhol succession. The conglomerates are sandy matrix-supported and they can be classified as debris flow deposits. They occur in 3 m to 20 m thick Incised-Valley-Fill alluvial fan successions below transgressive surface in the Asurkhol package (detail description in chapter 4)

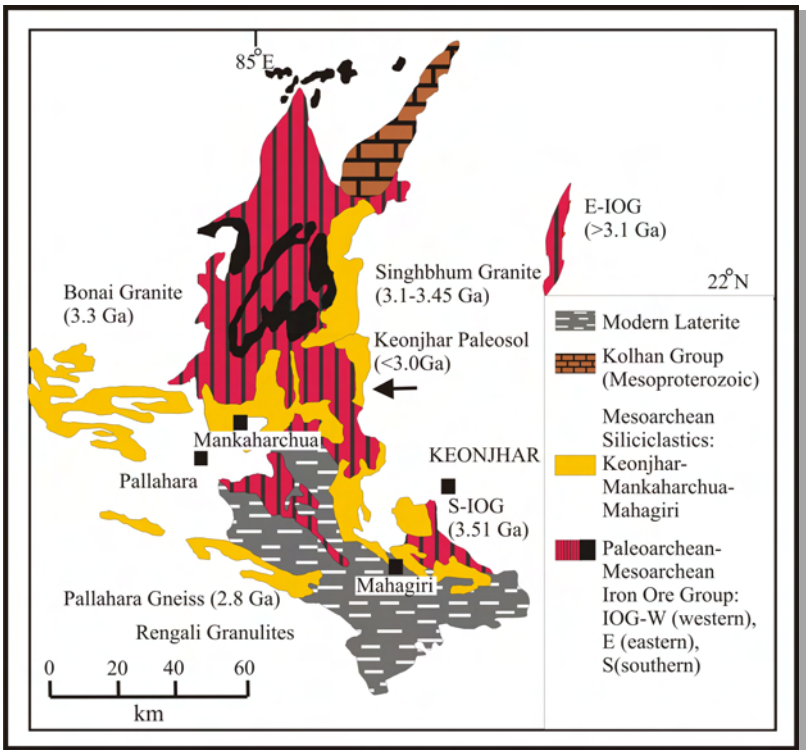

Fig. 7.1. Distribution of QPC (Quartz Pebble Conglomerate) bearing siliciclastic succession (Pallahara-Mankaharchua-Mahagiri-Keonjhar) of Singhbhum craton.

7.2. Sampling and analytical methods

The samples were collected from different QPC beds and medium-grained quartzarenites (Fig. 7.2; Appendix: A for location) and polished thin-sections were studied under RL-TL petrological microscope. SEM-EDS analysers were carried out using carbon coated thin section in the TESCAN VEGA-LSU scanning electron microscope (SEM) at the Presidency University. This instrument was commonly operated at 30 kV and a beam current of 10 nA. Back scattering electron (BSE) and secondary electron (SE) images were recorded in 22-25 mm working distance.

Major element analyses were carried out by using X-ray fluorescence spectrometry (XRF Model Panalytical Axios WD-XRF) at the Department of Geology, Presidency University. The pressed powder pellets were analysed on the XRF with matrix correction procedure at 60 kV, 170 mA with nominal analysis time was 300s for all major oxides (Table 7.1). Overall precision for major and minor

oxides is <5%. The overall accuracy (percent relative standard deviation [RSD]) for the major and minor oxides is 5%. The average precision is reported as better than 1.5% (Saini et al. 2000). The rock standard JG-2 (granite) and NIM G (granite) were used for the XRF analysis (Appendix B). Analyses trace element concentrations including REEs were carried out using Inductively Coupled Plasma Mass Spectrometry (ICPMS) at the ACME lab Canada (Table 7.2, 7.3). The precision and accuracy level were <5% RSD (Balaram and Rao 2003). The precision and accuracy are based on multiple analyses of international rock standards [JG-2 (granite), GSR-5 (shale)]. Results of analyses of the standard samples are given in (Appendix C).

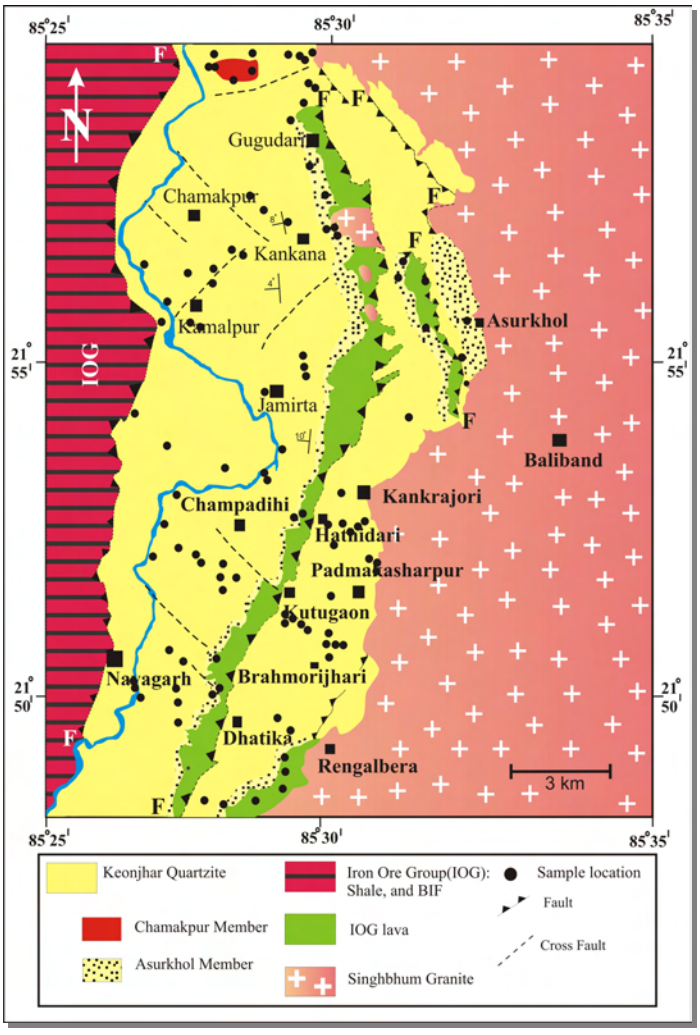

Fig. 7.2. Geological map of the Keonjhar Quartzite, north of Keonjhar with sample locations (dark filled circles) that are used for petrography and geochemistry.

7.3. Results

7.3.1. Petrographic and mineralogical compositions of the QPCs

7.3.1.1. Rutile

Most common heavy mineral present in the QPC matrix are Ti-bearing mineral phases of rutile (TiO_2). Rutile is identified by elongated prismatic shape (sometime irregular outline), yellow to brown weak pleochroism, high refractive index and relief. SEM-EDS composition of Ti-oxides show wide variation from pure TiO_2 to mixed Ti-bearing oxide phases with U and REE in composition (Fig. 7.3A, B) and are likely to represent intermediate phases such as leucoxene (discussed later in this chapter) in between rutile and brannerite. Rutile grains are also altered to Ca-U-Th phosphatic mineral phases at places (Fig. 7.3C).

A.

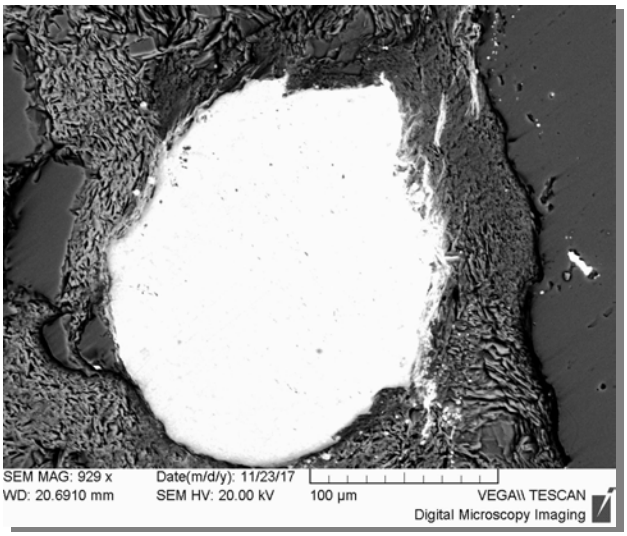

B.

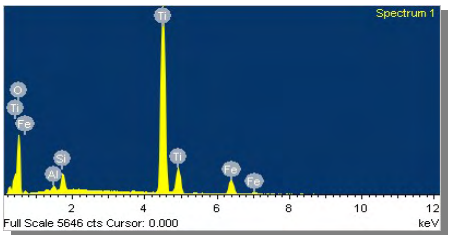

C.

Element	Weight %	Atomic %	Compd%	Formula
Al K	0.67	0.67	1.27	Al_2O_3
Si K	2.21	2.10	4.72	SiO_2
Ti K	50.59	28.28	84.39	TiO_2
Fe K	7.48	3.58	9.62	FeO
O	39.05	65.36		
Totals	100			

Fig. 7.3. SEM-EDS analysis from conglomerate (QPC) samples of Keonjhar Quartzite. A. SEM- BSE image of rutile grain. B. SEM-EDS analysis rutile grain. C. Semiquantitative analysis and compositional variation in rutile grain.

7.3.1.2. Brannerite

Brannerite is the most abundant U-bearing mineral phase identified from some QPC samples. It is isotropic with high reflectivity and euhedral outline. It is found within the clay pseudomatrix. SEM and EDS analyses suggest composition (Fig. 7.4A) that corresponds to generalized chemical formula of brannerite with variable Ca, Fe, Th and REE content e.g., $(U,Ca,Fe,Y,Th)_3\ Ti_5O_{14}$ (after De Voto 1978; Morton 1978). The uranium in brannerite is partly oxidized. The general chemical compositional range for brannerite is suggested as U_3O_8 (26-59.94%), ThO_2 (0.3-12.81%), TiO_2 (32-50%), CaO (0.1-3.38%), FeO (0.25-5.4%), RE_2O_3 (max 9.75%) (Saagar and Stupp 1983). The semiquantitaive EDS composition of the brannerite (Fig. 7.4B, C) in Keonjhar QPC is comparable to the generalized compositional range suggested by Saagar and Stupp (1983).

7.3.1.3. Uraniferous leucoxene

Leucoxene is a mixed U- bearing Ti mineral phase. This phase is identified within QPC pseudomatrix (Fig. 7.5 A, B) associated with clay minerals or rarely found in between two quartz grains. The compositional variation U_3O_8 = > 20% - <26%, ThO_2 = > 3.6%, TiO_2 = 50- 96.5%, CaO = 0.23 - 1.29% and FeO = 0.1 - 3.26%. The EDS composition of the leucoxene (intermediate phase between rutile and brannerite) (Fig. 7.5C) in Keonjhar QPC is comparable to the generalized compositional range suggested by Saagar and Stupp (1983).

Some of these grains show corona-like texture with brannerite overgrowth around rutile-core (Fig. 7.6 A, B). SEM-EDS line scan and element maps (Fig. 7.6C) reveal such zoned composition with higher U-concentration in the rims.

7.3.1.4. Coffinite

Coffinite (U $(SiO_4)_{1-x}$ $(OH)_{4x}$) is the other U-bearing phase identified from the Keonjhar QPC. Coffinite occurs as irregular body of microcrystalline uranium mineral phase (Fig. 7.7 A, B). In transmitted light it is opaque and in BSE images it appears as bright milky white in nature. The semiquantitative EDS chemical composition of coffinite suggests a compositional range of UO_3: 61.04%, SiO_2:28.67, P_2O_5: 8.42 and CaO: 1.87 (Fig. 7.7 C).

7.3.1.5. Thorite and Uranothorite

Thorite ($ThSiO_4$) and Uranothorite [$(Th,U)SiO_4$] occurs within QPC matrix exclusively as sand-sized and prismatic grains with sub-rounded (detrital) outline (Fig. 7.8 A, B). The semi quantitative EDS analysis suggests ThO_2 varying between 39.74-50.54% (Fig. 7.8 C). The other components are Al, Si, P, Ca, Fe and LREE (mainly La and Ce). The SEM-EDS study further shows compositional (semi quantitative) ranges of other oxides: Al_2O_3: 1.33-8.33%, SiO_2:17.87- 34.39%, P_2O_5: 3.15-15.63%, CaO: 1.61-3.61%, FeO: 1-1.67%, La_2O_3: 0.12-0.38% and Ce_2O_3: 1.45-1.91%.

7.3.1.6. Pyrite

Pyrite is identified under reflected light by its golden colour, isotropic nature, high reflectivity, partially preserved octahedral habit (Fig. 7.9 A). The detrital nature and the effect of mechanical transport is confirmed by smooth and rounded outline, broken, abraded and ground boundaries of the pyrite grains. EDS compositions were obtained from SEM studies (Fig. 7.9 B, C and D).

A.

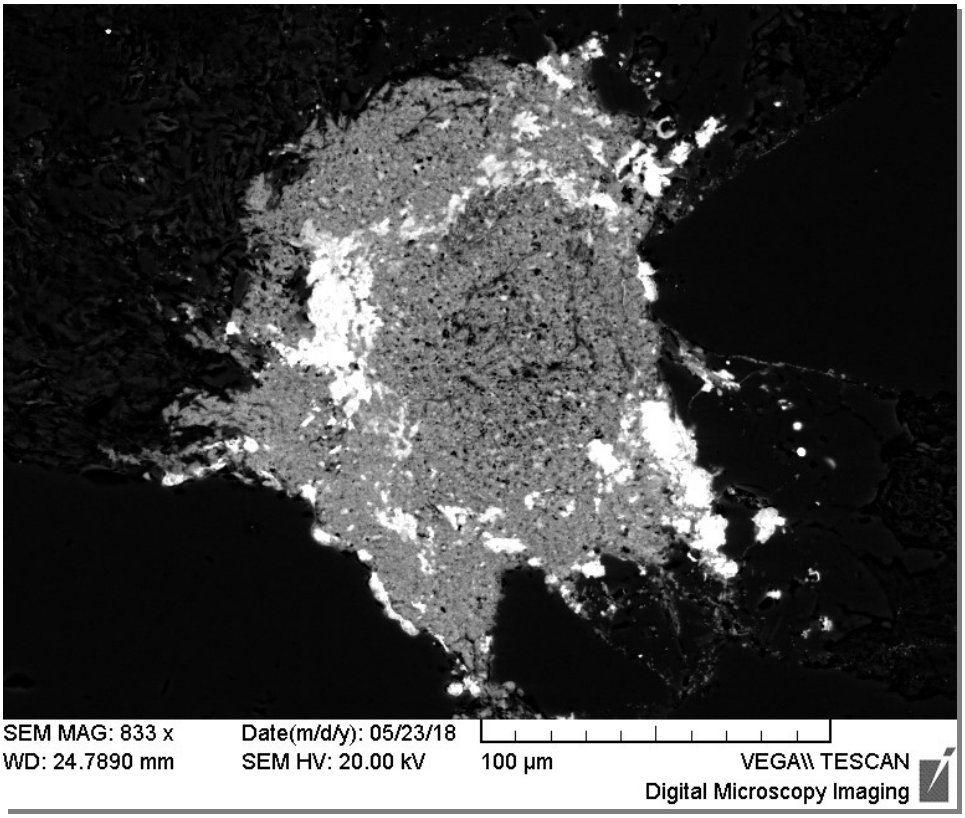

B.

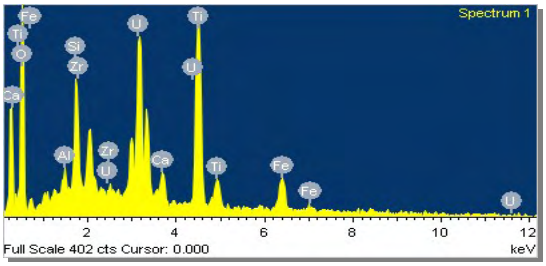

C.

Element	Weight%	Atomic%	Compd%	Formula
Al K	0.94	1.22	1.78	Al_2O_3
Si K	4.60	5.74	9.84	SiO_2
Ca K	1.93	1.69	2.71	CaO
Ti K	19.84	14.52	33.10	TiO_2
Fe K	5.39	3.38	6.94	FeO
Zr L	7.48	2.87	10.10	ZrO_2
U M	29.57	4.35	34.81	U_3O_8
O	30.24	66.22		
Totals	100.00			

Fig. 7.4. SEM-EDS analysis from conglomerate (QPC) samples of Keonjhar Quartzite. A. SEM- BSE image of brannerite grain. B. SEM-EDS analysis brannerite grain. C. Semiquantitative analysis and compositional variation in brannerite grain.

A.

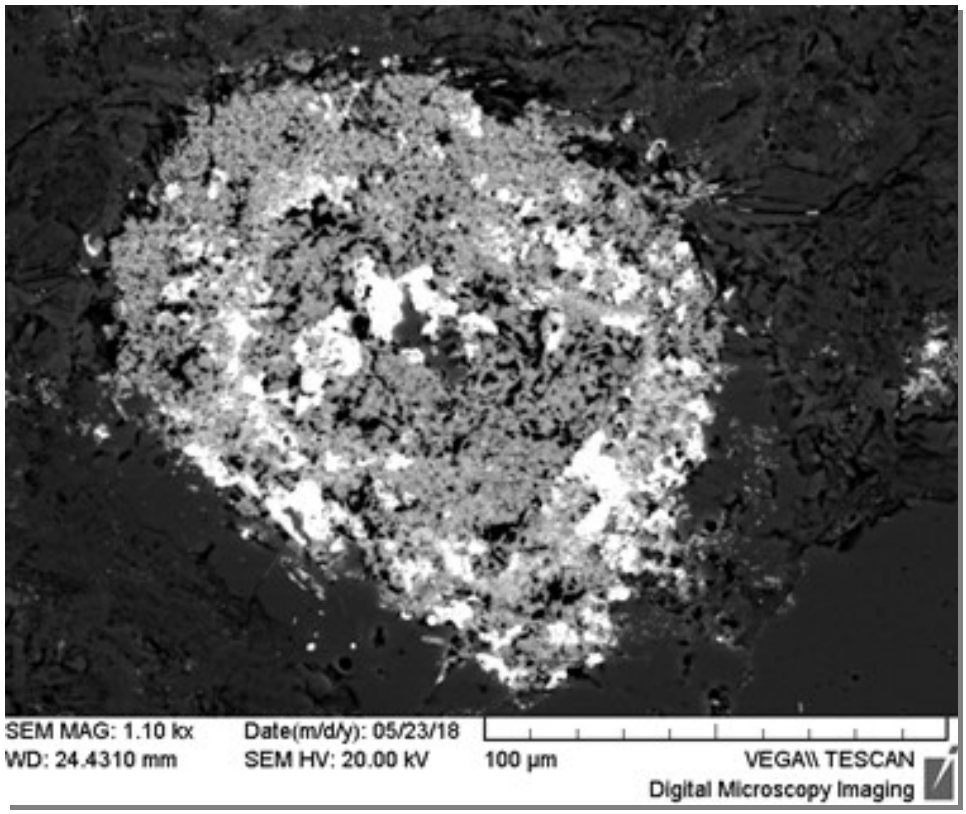

B.

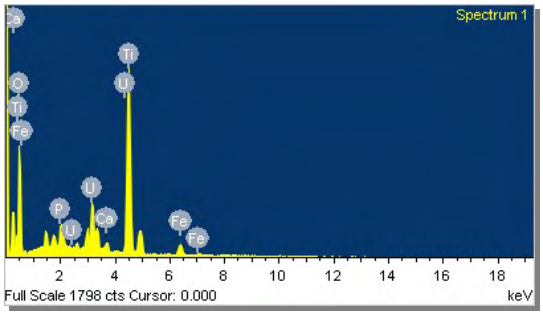

C.

Element	Weight%	Atomic%	Compd%	Formula
P K	1.92	1.91	4.39	P_2O_5
Ca K	1.07	0.82	1.49	CaO
Ti K	40.30	25.90	67.22	TiO_2
Fe K	4.42	2.43	5.68	FeO
U M	17.65	2.28	21.52	U_3O_8
O	34.65	66.66		
Totals	100.00			

Fig. 7.5. SEM-EDS analysis from conglomerate (QPC) samples of Keonjhar Quartzite. A. SEM- BSE image of uraniferous leucoxene grain. B. SEM-EDS analysis uraniferous leucoxene grain. C. Semiquantitative analysis and compositional variation in uraniferous leucoxene grain.

A.

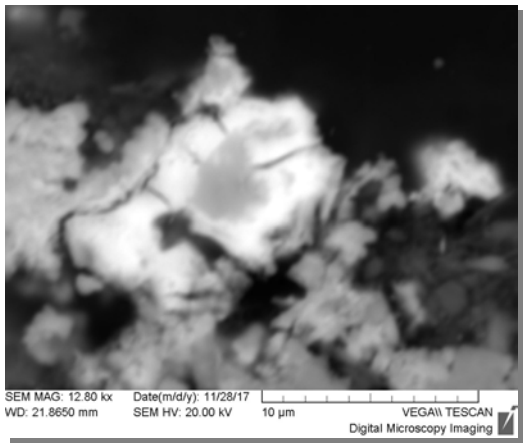

B.

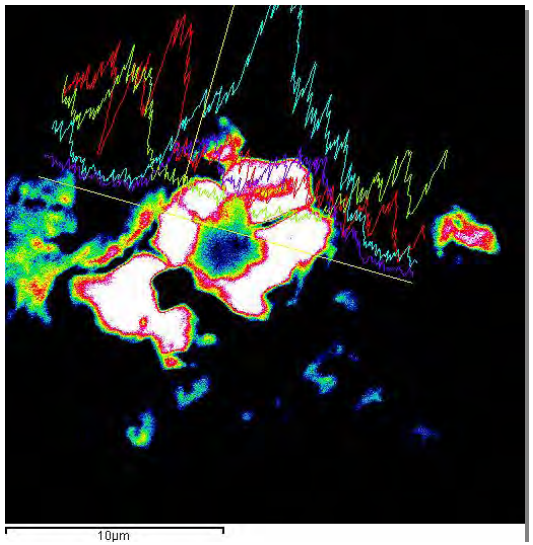

C.

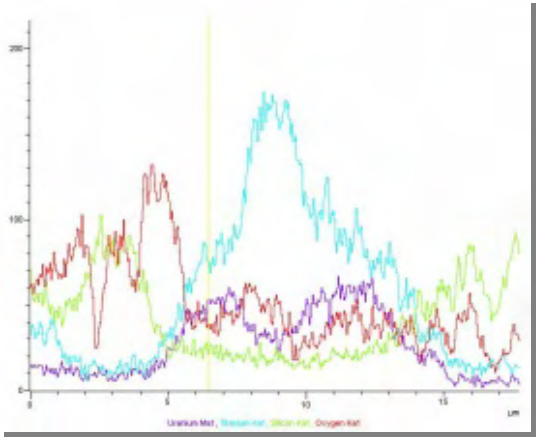

	Rutile	Leucoxene	Brannerite
Oxides		Compd%	
SiO_2	2.79	3.45	26.07
P_2O_5	1.86	3.87	4.5
CaO	0.89	1.2	1.79
TiO_2	82.33	69.05	31.05
FeO	3.9	5.01	5.98
U_3O_8	7.08	17.06	29.98

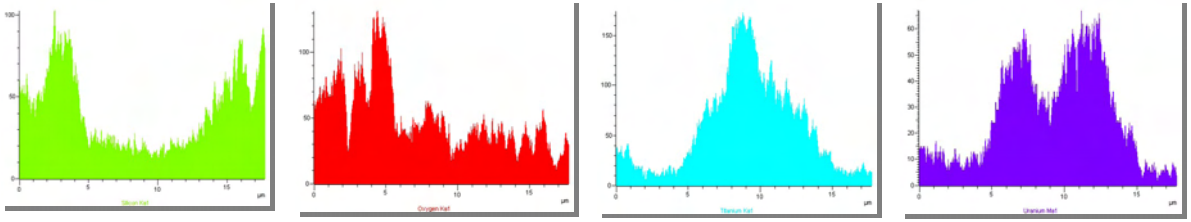

Fig. 7.6. SEM- EDS images and analyses of corona texture A. SEM image showing corona texture (rutile in the core and brannerite in the rim) from Pronto Reaction. B. SEM-EDS image of elemental map. C. Line scan map and semiquantitative analysis of the core to rim corona texture.

7.3.1.7. Monazite

This mineral is commonly occurring as euhedral grain and present within QPC matrix (Fig. 7.10A, B). Mineral phase is characterized by high concentration of REE (Ce, La, Y and Nd) PO_4 (Fig. 7.10C). Ce-Monazite is mainly recognized with trace amount of Th and U which indicates the primary nature of monazite. These minerals are present within the pseudomatrix. Primary monazite formed mainly in the grain boundary of framework grain and matrix.

7.3.1.8. Zircon

Zircon occurs as prismatic or variably rounded (Fig. 7.11 A, B) detrital grains. Zircon is identified by the high relief, high birefringence and blunt elliptical or subhedral prismatic grains, higher order interference colour. At some places of the QPC the zircons are prismatic shape with oscillatory zoning (Fig. 7.11 C). Oscillatory zoned band thickness varies from thick to thin. In some region showing high degree of alteration and metamictization within the zircon grains can be identified by patchy distribution.

7.3.2. Provenance and tectonic setting of the source terrain from geochemical studies

The chemical composition of the sediments is closely related to the tectonic settings. This compositional distribution helps to identify the source rock. Major oxides composition of sediments and that of source rocks do not correlate entirely, as weathering in the source region may lead to compositional changes. Trace elements as well bear a relationship to the composition of the source terrain. The major and trace element concentrations of QPC, sandstone, mudstone and shale samples are reported in Tables 7.1, 7.2 and 7.3. QPCs and host sandstones are enriched in SiO_2 (94% –98.2

wt %) and depleted in Na_2O (0.01–0.11 wt %), CaO (0.01–0.03 wt %), and TiO_2 (0.02–0.45 wt %).

A.

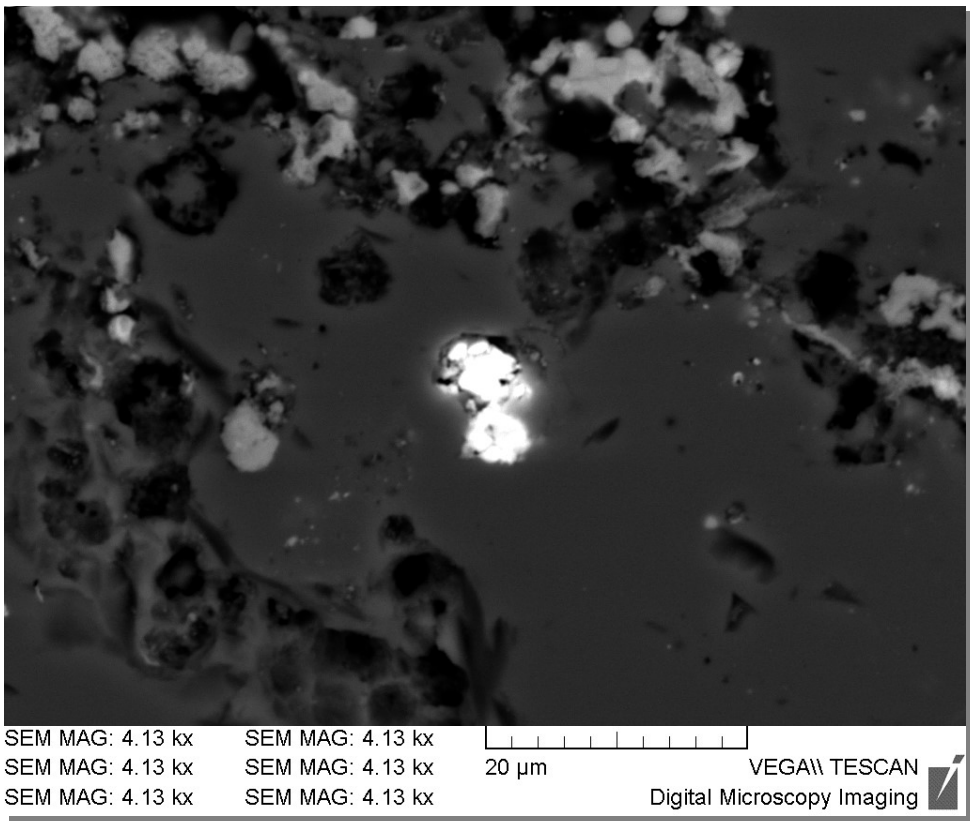

B.

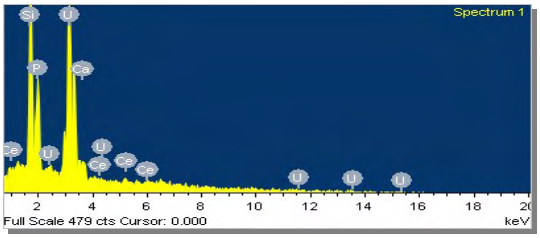

C.

Element	Weight%	Atomic%	Compd%	Formula
Si K	15.01	17.88	32.11	SiO_2
P K	4.85	5.24	11.11	P_2O_5
Ca K	1.40	1.17	1.96	CaO
Ce L	0.83	0.20	0.97	Ce_2O_3
U M	44.81	6.30	53.85	UO_3
O	33.10	69.22		
Totals	100.00			

Fig. 7.7. SEM-EDS analysis from conglomerate (QPC) samples of Keonjhar Quartzite. A. SEM- BSE image of coffinite grain. B. SEM-EDS analysis coffinite grain. C. Semiquantitative analysis and compositional variation in coffinite grain.

A.

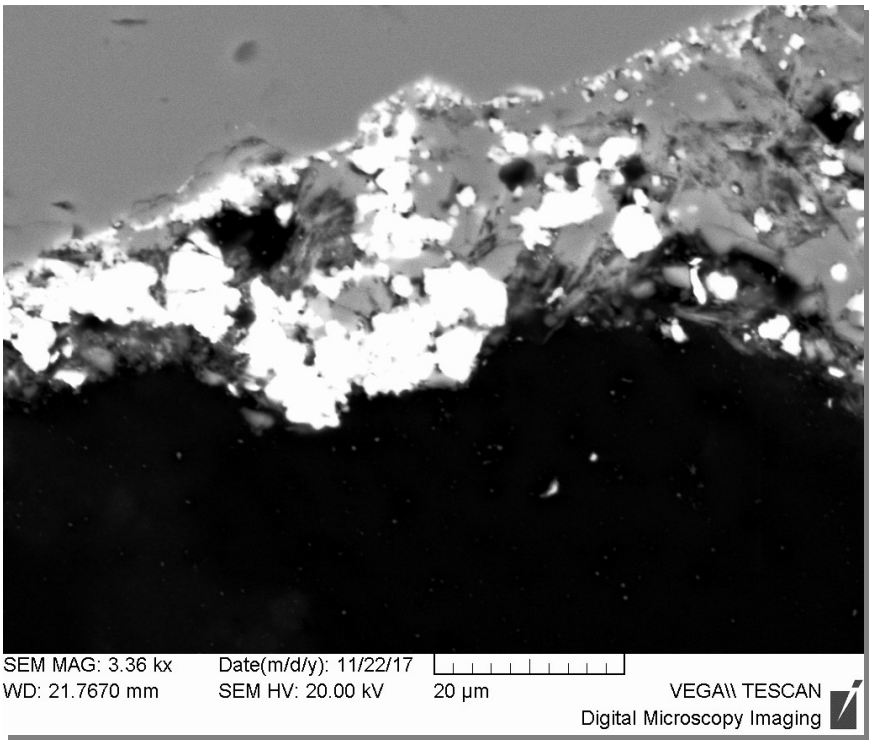

B.

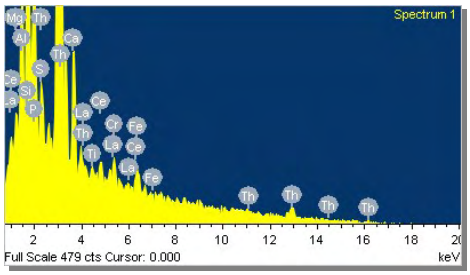

C.

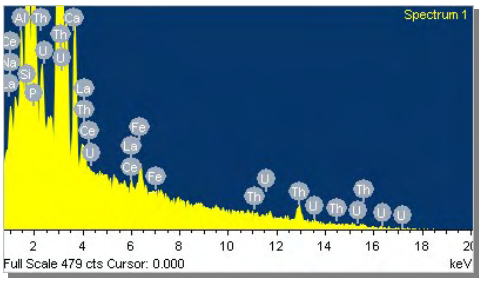

D.

Element	Weight%	Atomic%	Compd%	Formula
Mg K	0.39	0.49	0.65	MgO
Al K	2.87	3.25	5.42	Al_2O_3
Si K	16.08	17.47	34.39	SiO_2
P K	4.69	4.62	10.76	P_2O_5
S K	0.45	0.43	1.13	SO_3
Ca K	2.06	1.57	2.89	CaO
Ti K	0.21	0.14	0.35	TiO_2
Cr K	0.81	0.47	1.18	Cr_2O_3
Fe K	0.91	0.50	1.17	FeO
La L	0.34	0.08	0.40	La_2O_3
Ce L	1.63	0.35	1.91	Ce_2O3
Th M	34.92	4.59	39.74	ThO_2
O	34.62	66.04		
Totals	100.00			

Fig. 7.8. SEM-EDS analysis from conglomerate (QPC) samples of Keonjhar Quartzite. A. SEM- BSE image of thorite and uranothorite grain. B. SEM-EDS analysis thorite grain. C. Semi quantitative analysis and compositional variation in thorite grain and D. Uranothorite composition.

A.

B.

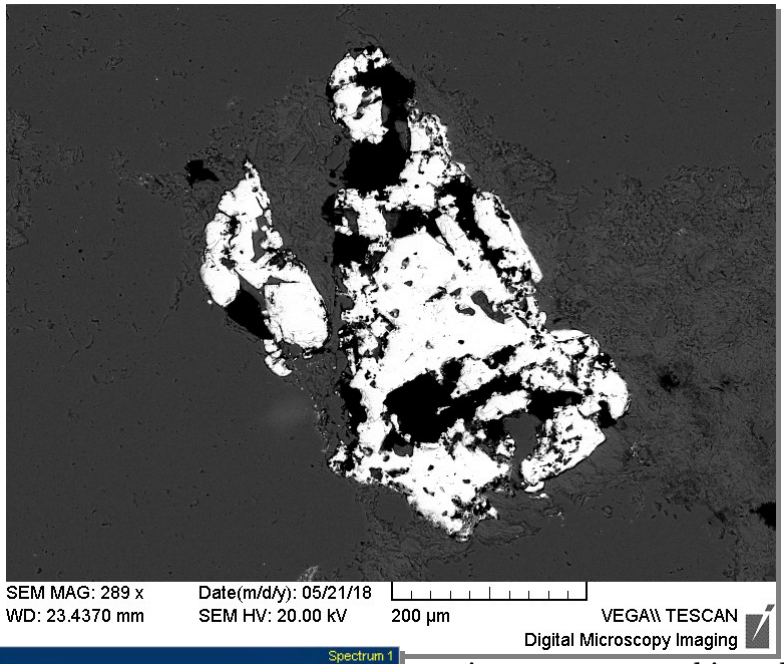

C.

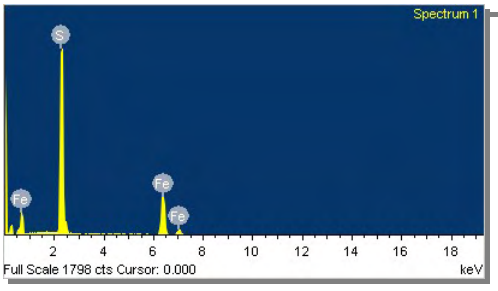

D.

Element	Weight%	Atomic%	Compd%	Formula
S K	28.51	20.40	71.18	SO_3
Fe K	22.40	9.20	28.82	FeO
O	49.09	70.40		
Totals	100.00			

Fig. 7.9. Petrographic and SEM-EDS analysis from conglomerate (QPC) samples of Keonjhar Quartzite. A. RL image of the pyrite grain. B. SEM- BSE image of pyrite grain. C. SEM-EDS analysis pyrite grain. D. Semiquantitative analysis and compositional variation in pyrite grain.

A.

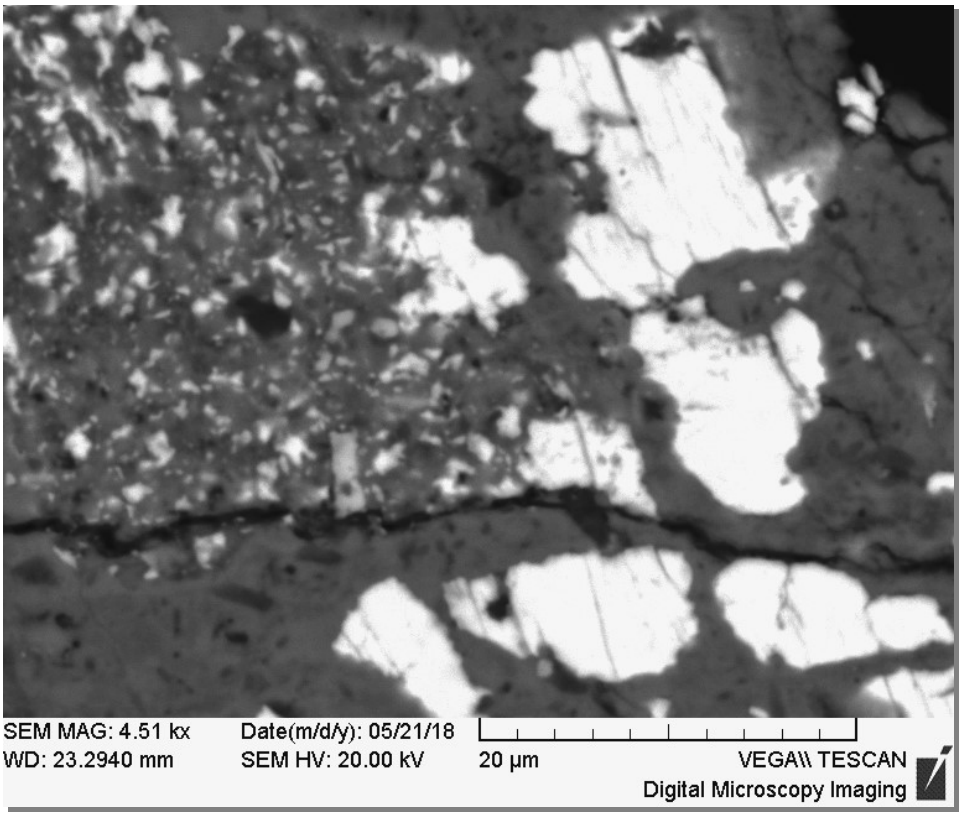

B.

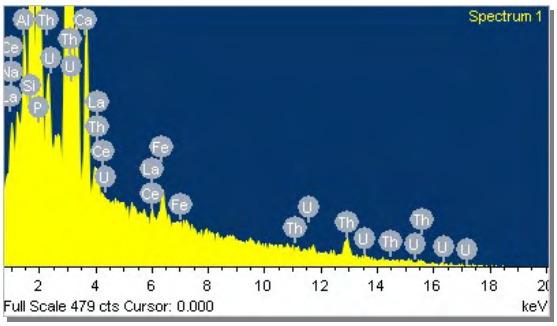

C.

Element	Weight%	Atomic%	Compd%	Formula
P K	8.79	6.54	33.87	P_2O_5
La L	10.01	1.66	19.73	La_2O_3
Ce L	17.31	2.84	34.07	Ce_2O_3
Nd L	3.84	0.61	7.53	Nd_2O_3
Th M	2.51	0.25	4.81	ThO_2
O	46.48	66.90		
Totals	100.00			

Fig. 7.10. SEM-EDS analysis from conglomerate (QPC) samples of Keonjhar Quartzite. A. SEM- BSE image of monazite grain. B. SEM-EDS analysis monazite grain. C. Semiquantitative analysis and compositional variation proportion of monazite grain.

A.

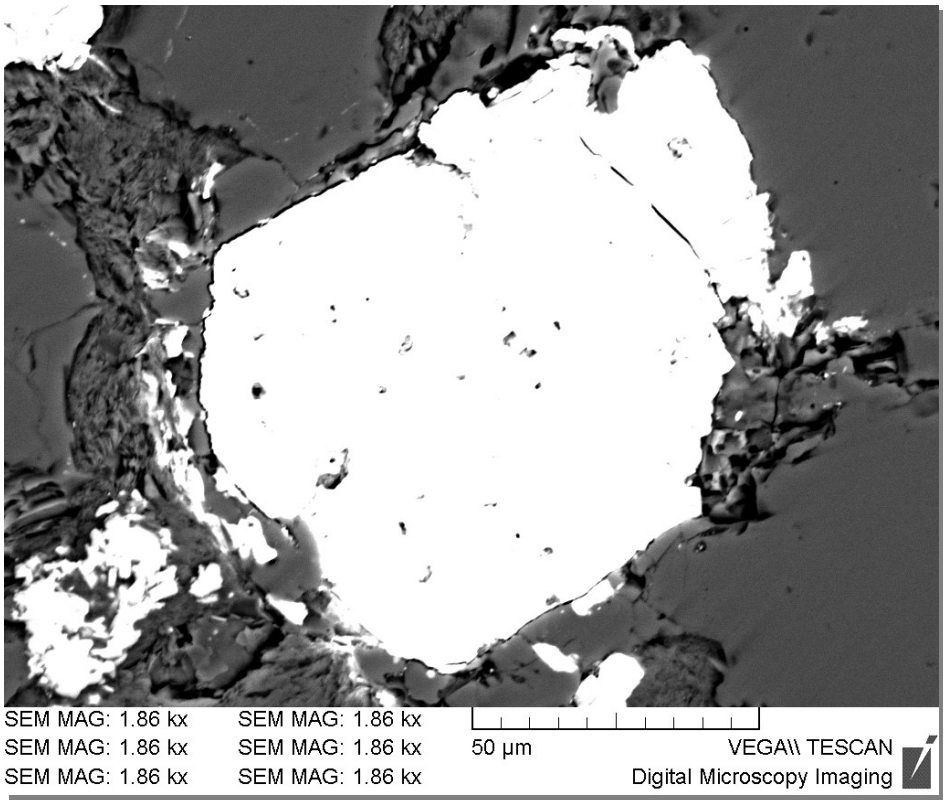

B.

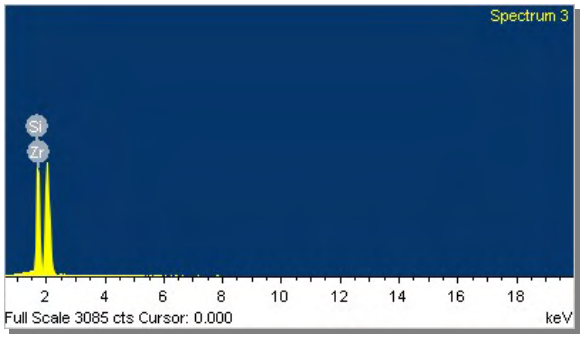

C.

Element	Weight%	Atomic%	Compd%	Formula
Si K	14.27	15.80	30.53	SiO_2
Zr L	51.43	17.53	69.47	ZrO_2
O	34.30	66.67		
Totals	100.00			

Fig. 7.11. SEM-EDS analysis from conglomerate (QPC) samples of Keonjhar Quartzite. A. SEM- BSE image of zircon grain. B. SEM-EDS analysis zircon grain. C. Semiquantitative analysis and compositional variation in zircon grain.

7.3.2.1. Spider plots

7.3.2.1.1. Incompatible elements

QPC and sandstone-mudstone samples are depleted in Sr, Cr, Ni, Rb, Cs, Ba, and Pb compared with the Archean upper crust (AUC) (values after Taylor and McLennan 2009) (Fig. 7.12, 7.13). Zr and Hf concentrations of the QPCs are comparable to AUC (Fig. 7.12, 7.13). Th and U contents are also consistent or similar for sandstone and mudstone (Table 7.2) and are slightly enriched in QPC with respect to the AUC. Samples show a weak to strong negative Nb anomaly compared with AUC (Fig. 7.12, 7.13). All of the QPC samples are depleted in Sr, Cr and Ni and enriched in Ta anomaly with respect to the AUC. The Y anomaly of all the Keonjhar samples is similar to that in the AUC.

7.3.2.1.2. Compatible elements

The sandstones are somewhat depleted in compatible elements and QPCs show enrichment of Co and depletion in Cr (Appendix D, Fig. 7.12, 7.13). The concentrations of Sc and V in mudstone are similar and slightly depleted to the AUC. LIL elements such as Rb, Cs, Sr, Ba and Pb tend to substitute for K, because of their large radii and low electrical charges and hence are concentrated in felsic rather than mafic rocks (Mason and Moore 1982). Rb and Cs are preferentially retained in the weathering profile by adsorption or exchange onto the illite rich clays (Butler 1954; Nesbitt et al. 1997; Ali et al. 2014). Enrichment of LIL elements may suggest a predominantly felsic source whereas depletion suggests input from undifferentiated source rocks (Ghosh et al. 2016). Enrichment of compatible elements and/or depletion in HFSE and LIL elements is indication some input from the mafic rocks as well (cf. Ghosh et al. 2016).

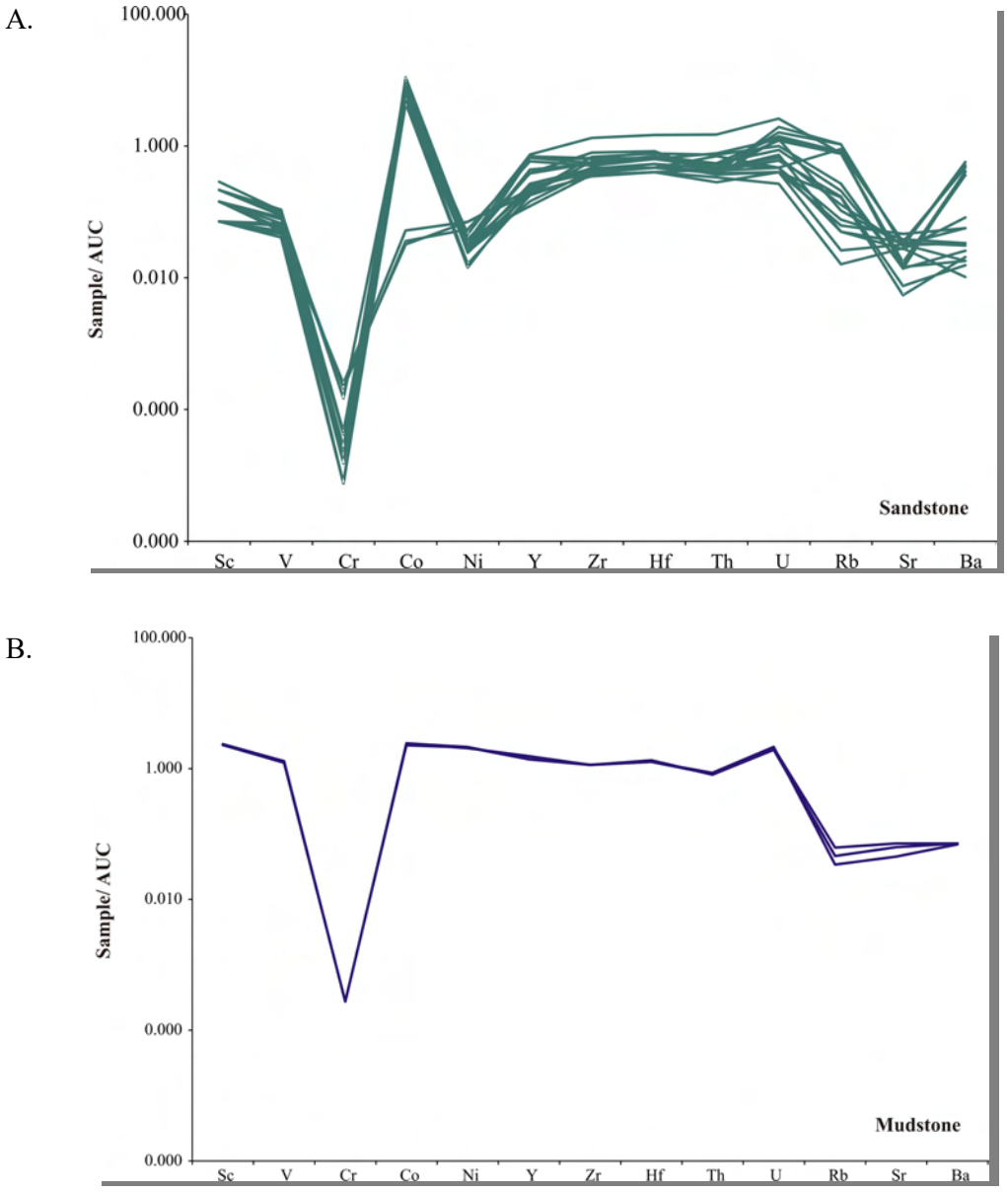

Fig.7.12. Plots of trace elements data normalized with Archean upper crust (AUC) from the Keonjhar Quartzite. A. Trace element composition of arenites normalized to Archean upper crust (AUC). B. Trace element composition of mudstones normalized to Archean upper crust (AUC).

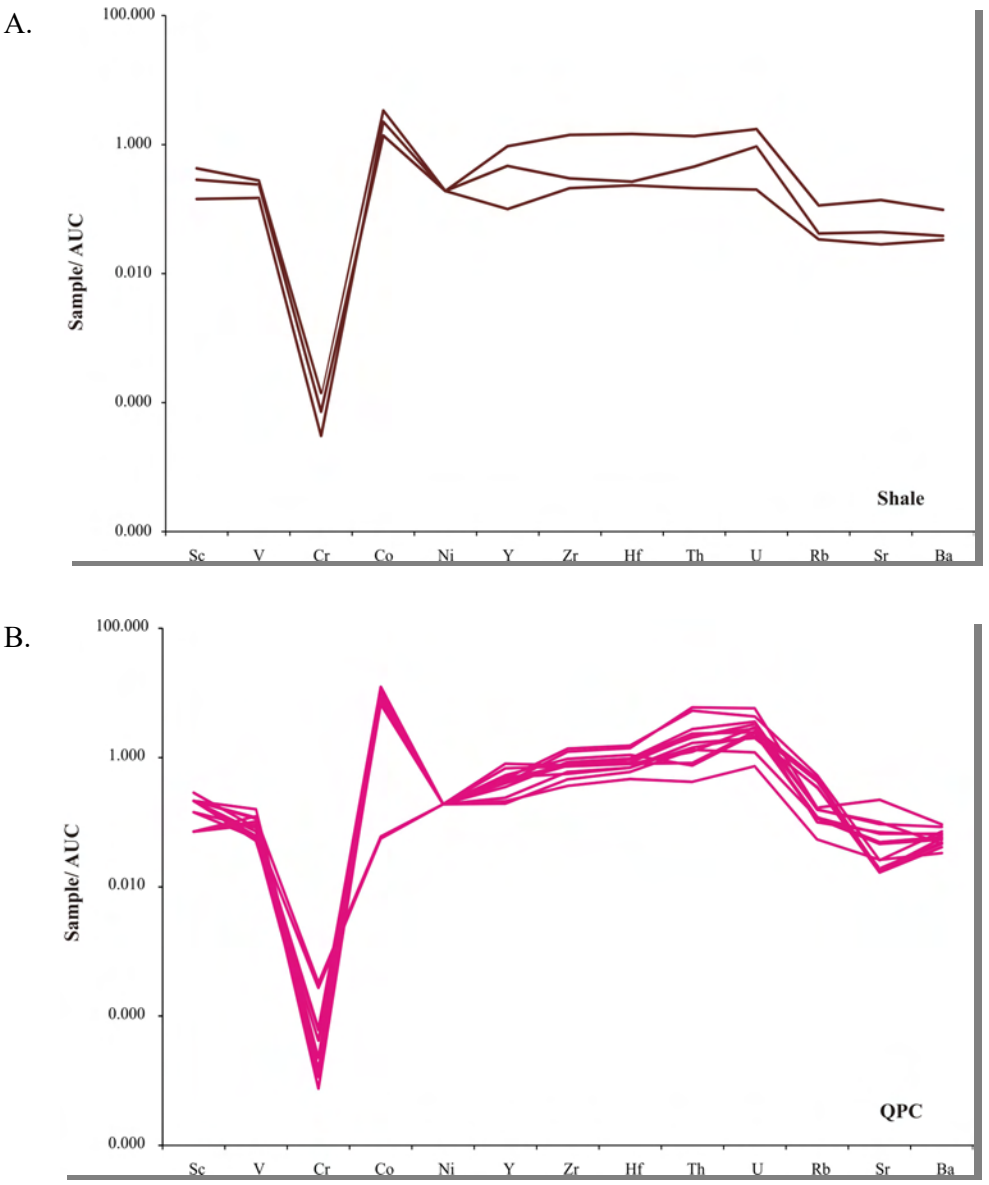

Fig.7.13. Plots of trace elements data normalized with Archean upper crust (AUC) from the Keonjhar Quartzite. A. Trace element composition of shale normalized to Archean upper crust (AUC) B. Trace element composition of QPCs normalized to Archean upper crust (AUC).

7.3.2.2. *Th/Sc and Zr/Sc* bivariate diagram

The Th/Sc ratio is an indicator of igneous chemical differentiation process because Th is typically an incompatible element, whereas the Sc is a typically compatible

element in magmatic crystallization system. On the other hand Zr/Sc is a useful index for zircon enrichments. McLennan et al. (1993) suggested that trace element composition of sedimentary rocks are likely to be controlled by detrital Zircon and monazite content. Only zircon is visible from the Keonjhar samples.

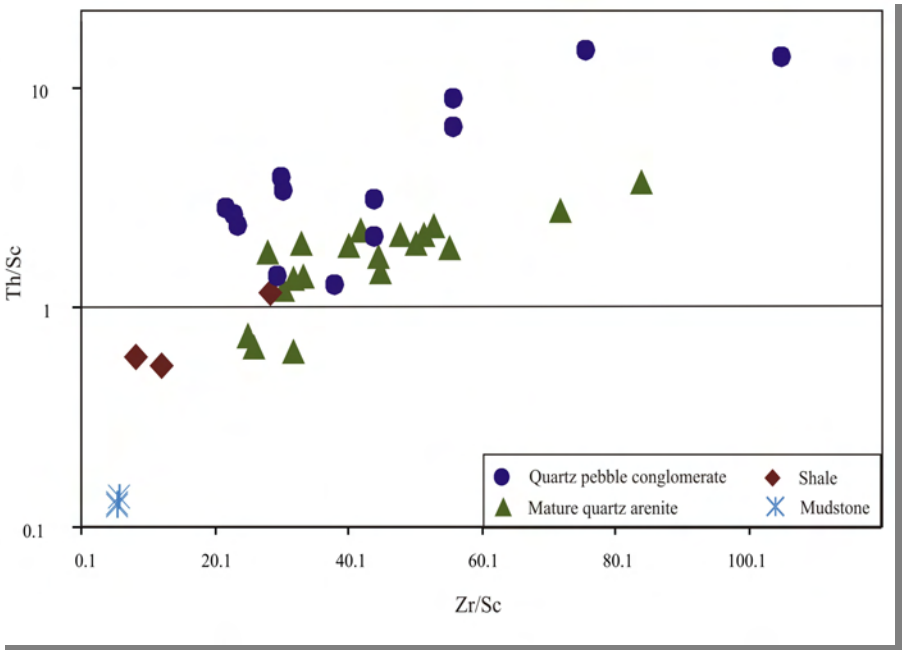

Fig.7.14. Plot of Th/Sc versus Zr/Sc for the Mesoarchean Keonjhar Quartzite samples. Note wide range in Zr/Sc value for both QPCs and sandstones. A relatively positive correlation with Th/Sc values with all the samples.

Zircon concentration in Keonjhar samples is represented in Th/Sc and Zr/Sc variation diagram (Fig.7.14) (fields after McLennan et al. 1993). Th/Sc and Zr/Sc variation diagram reflects compositional variation trend. High variability in Th/Sc ratio indicates that the samples show influence of both felsic as well as mafic source. Shale and mudstone samples have values for both ratios (Th/Sc and Zr/Sc) low, but QPC and mature quartz arenite are showing high contains of Th and Zr with high Zr/Sc range suggesting higher degree of sorting and recycling.

7.3.2.3. Cr/Th versus. Sc/Th

Cr is susceptible to the effects of weathering and sedimentation, the Cr/Th ratio in sediments may not monitor sedimentary provenance. It is plotted against Sc/Th (after Condie and Wronkiewicz 1990, Fig. 7.15) in three mudstones and samples are showing strong positive correlation Cr/Th with Sc/Th. Similar correlations ar not observed in case of other samples. Low and almost constant Sc/Th value suggests enrichment of Cr in some quartz arenite samples are related to sedimentary processes and does not bear signature of provenance.

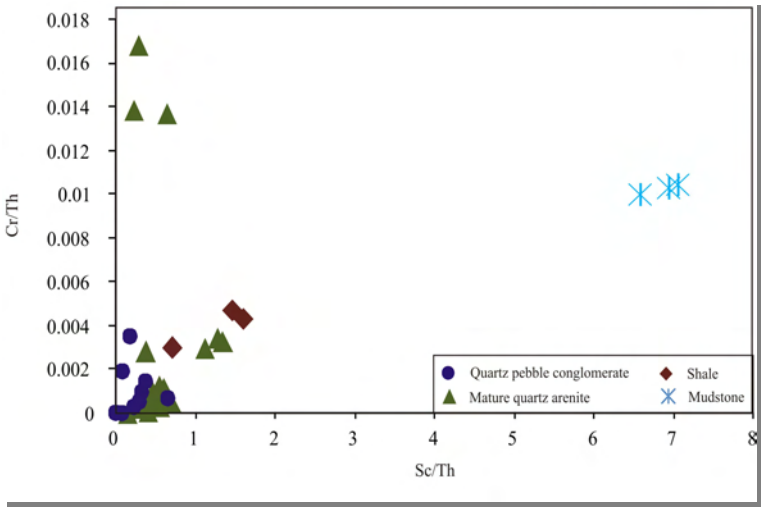

Fig.7.15. Plot of Cr/Th versus Sc/Th for the Mesoarchean siliciclastics samples. Note. Cr/Th does not show strong positive correlation trend with Sc/Th ratio.

7.3.2.4. Cr/V versus. Y/Ni

In Cr/V versus Y/Ni binary diagram, the Cr/V ratio denotes the index of enrichment of Cr over the other ferromagnesian trace elements, whereas Y/Ni monitors the general level of ferromagnesian trace elements (Ni) compared to a proxy for HREE (Y). In this diagram (Fig. 7.16A), mature quartz arenite samples show wide variation in Y/Ni that suggests a mixed source. QPC samples are generally showing low Y/Ni that is indicative of a mafic source. Cr/V varies and generally high in quartz arenite samples. It indicates enrichment of Cr over V.

A.

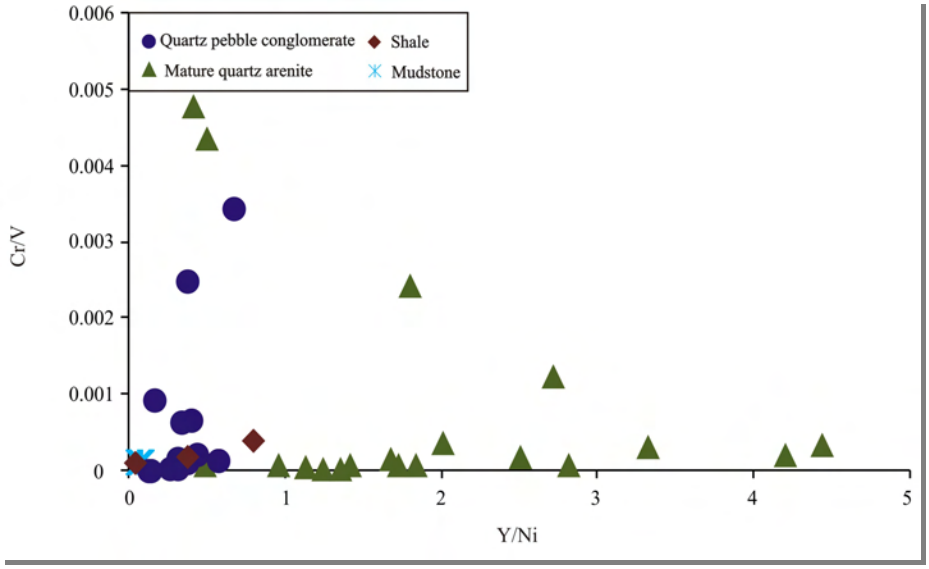

B.

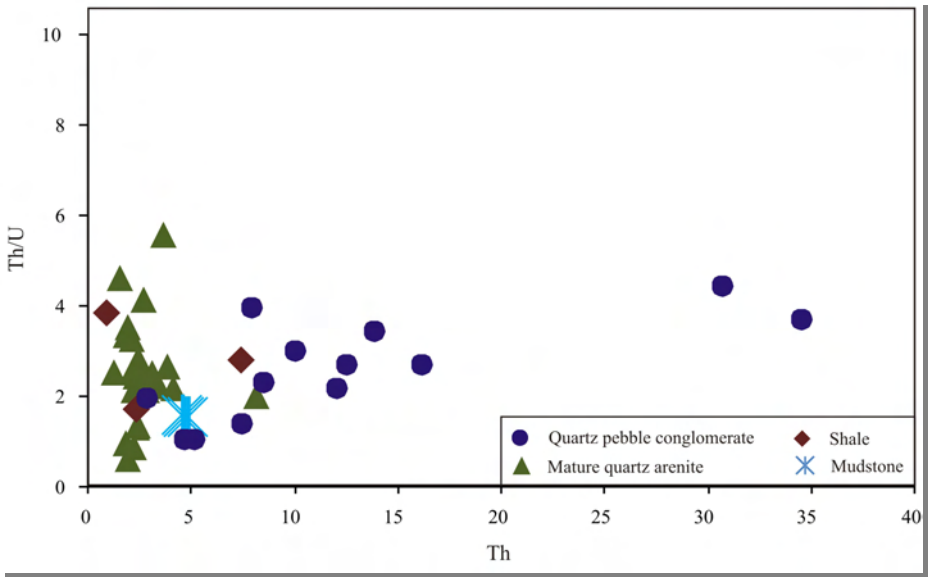

Fig. 7.16 A. Plot of Cr/V versus Y/Ni for the Keonjhar Quartzite samples. Note. Cr/V and Y/Ni ratio are showing a wide variation trend. B. Plot of Th/U versus Th for the Mesoarchean siliciclastic samples from the Keonjhar area. Note. Th/U and U proportion show wide range of variation.

7.3.2.5. Th/U-Th

The Th/U ratio in most upper crustal rocks is typically between 0 and 4.0 (McLennan et al. 1993). The ratio of Th/U shows wide spread in QPC and in mature quartz arenite and shale varies from 0.75 to 5.7. High Th/U > 4.5 (Bhatia and Taylor 1981) indicates weathering and sedimentary recycling due to loss of U, whereas low

values may suggest mantle derived sources depleted in LIL elements / absence of intense weathering. Highly reduced sedimentary environments can have enriched U leading to low Th/U ratios (Fig. 7.16B). On the other hand low to high Th/U ratio at a similar Th content for some sandstone and QPC samples (Fig. 7.16B) indicate preferential loss of U during diagenesis or subsequent weathering suggesting the presence of oxygen.

7.3.2.6. La-Th-Sc and Th–Sc–Zr/10

Trace elements such as La, Th, Sc, Co and Zr are transferred into clastic sediments during primary weathering due to their low mobility. Thus they are useful tool for provenance and tectonic discrimination (Bhatia 1985; Taylor and McLennan 1985; Taylor and McLennan 2009; Bhatia and Crook 1986).

La-Th-Sc (Fig. 7.17A) discrimination plots of Bhatia and Crook (1986) has been used to characterize the tectonic setting. In the La-Th-Sc diagram, maximum samples plots are closer to the La-Th join due to high concentration of La and Th. From this diagram it is typically granitic gneissic source. Many of the samples plot on the active continental margin and passive margin. In the La-Th-Sc ternary diagram, no discrimination between passive and active continental margin can be observed.

In the Th–Sc–Zr/10 diagram (Bhatia and Crook 1986; Fig. 7.17B), plots are parallel to the Th–Zr/10 join possibly because of high Zr content. QPC samples are close to Th point and fall in the field of active continental margin. The quartz arenite samples fall within the field of passive continental margin. Others samples are widely distributed, due to comparatively low contains of Th and Zr. In the present study, this diagram fails to differentiate between active and passive continental margin settings possibly because of varying proportion of Zr and Th in different samples.

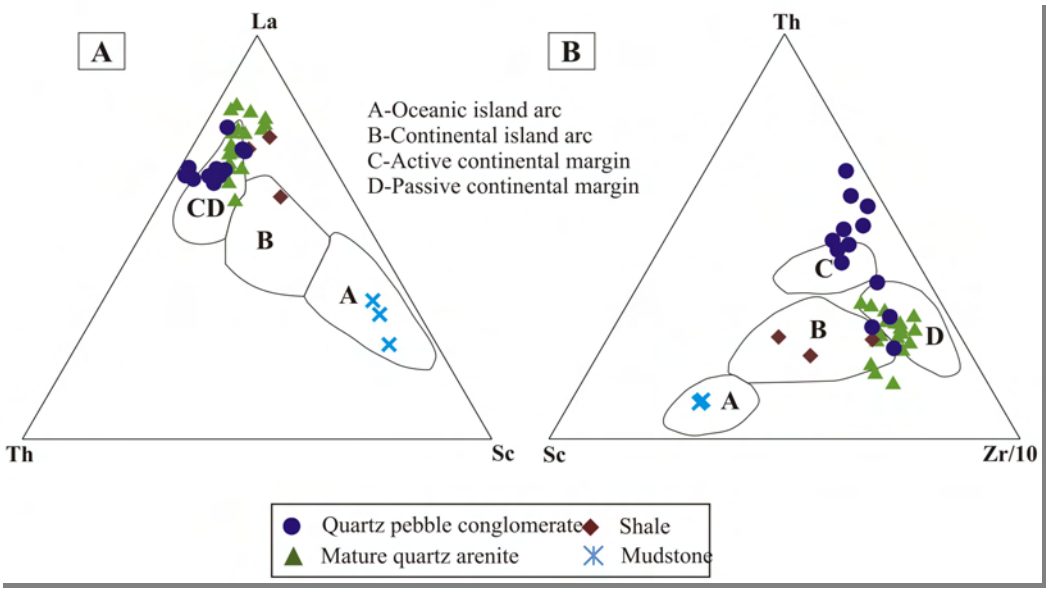

Fig.7.17 A. La–Th–Sc discriminatory plot (after Bhatia and Crook 1986). Note samples fall mainly in passive and active continental margin settings and a few in the oceanic island arc setting. B. Th–Sc–Zr/10 discriminatory plot (after Bhatia and Crook 1986). Note that most of the samples plot within and close to the fields of both active and passive continental margins and three samples of this formation plot in the field of oceanic island arc.

7.3.2.7. REE distribution patterns

Rare Earth Elements (REE) are good indicators for provenance. Trace elements do not fit readily into the crystallographic framework of most diagnostic minerals, but can be added as adsorbed particles on clay mineral surfaces, or included in interlayer cation sites and therefore ratios of low solubility trace elements in mudstones reflect those of source rocks (McLennan and Taylor 1991; Taylor and McLennan 2009). Many trace elements including the rare earth elements are transferred from source to sediments without significant fractionation and preserve the signature of the parent materials (Taylor and McLennan 1985, 2009). Hence, trace elements as compared to

major elements are expected to be more useful in discriminating tectonic environments and source rock.

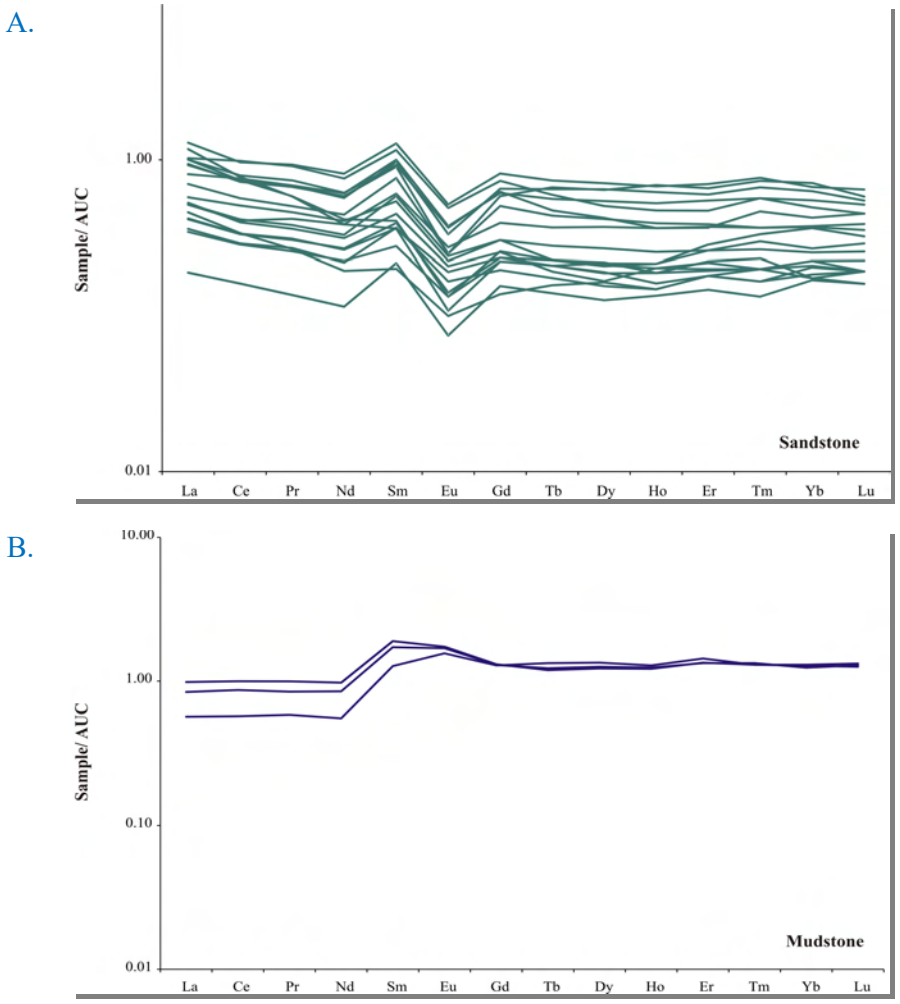

Fig.7.18. Plots of Rare Earth Element (REE) composition normalized to Archean upper crust (AUC): A. sandstone, note positive LREE and flat HREE distribution pattern and negative Eu anomaly, B. mudstone, note enrichment of HREE and flat LREE distribution pattern and positive Eu anomaly.

AUC normalized REE distribution pattern (Fig.7.18, 7.19) of sandstones reveal Negative Eu anomaly, positive LREE and flat HREE distribution pattern. Mudstone samples reveal positive Eu anomaly and HREE and flat LREE distribution pattern. Shale samples show positive Sm and negative Eu anomaly, flat LREE and HREE distribution pattern and slightly depleted in Ce anomaly. QPC samples show negative

Eu anomaly, positive LREE and flat HREE distribution pattern. The AUC normalized plot for all the samples from Keonjhar Quartzite reflect that it similar to the post Archean shales with enrichment of LREE and depletion of Eu anomaly.

A.

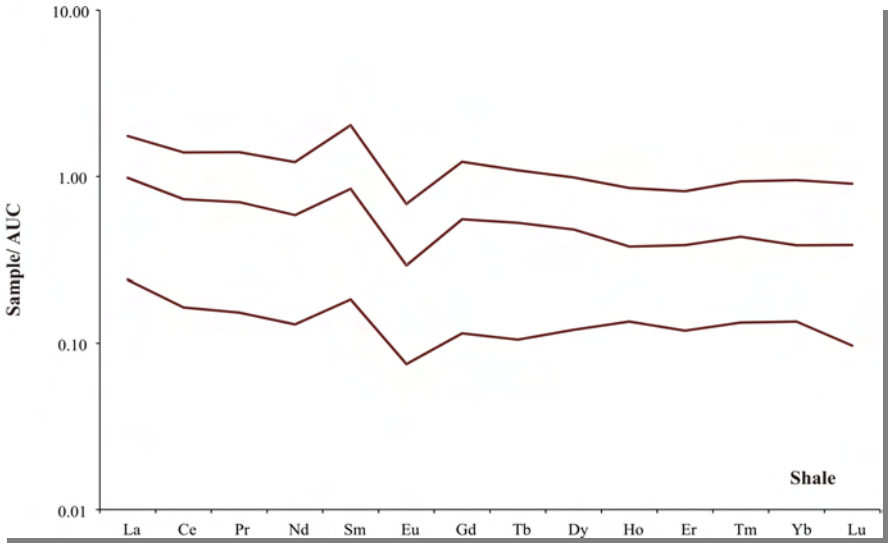

B.

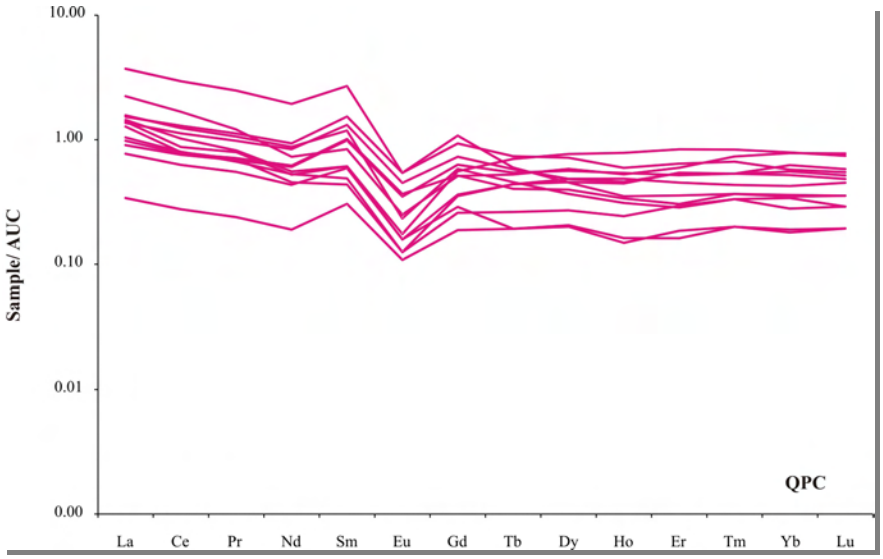

Fig.7.19. Plots of Rare Earth Element (REE) composition normalized to Archean upper crust (AUC): A. shale, note flat LREE and HREE distribution pattern, positive Sm and negative Eu anomaly and slightly depleted Ce anomaly, B. QPC. Note. Positive LREE and flat HREE distribution pattern, negative Eu anomaly.

7.3.3 Comparative account of chemical compositions of the QPCs, sandstone (quartzite)

In this section I present a comparative account of chemical compositions of the QPCs, sandstone (quartzite) in order to explore possible geochemical signals that might exist due to preferential concentration of radioactive minerals in the QPCs. I have also compared the composition of QPCs with composition of Singhbhum Granite to assess the source to sink differentiation of element composition that could be of importance for tracing the radioactive mineral potential of the QPCs. For the purpose of comparison I have normalized QPC compositions with respect to average sandstone composition of the Keonjhar Quartzite reported in this study (Table 7.1, 7.2 and 7.3) and average composition of Singhbhum Granite from published database (Appendix D; Saha 1994; Dey et al. 2017).

7.3.3.1. Keonjhar Sandstone normalized diagram

Major oxide, Trace and REE compositions of the sandstones and QPCs from the Keonjhar Quartzite have been reported in (Table 7.1, 7.2 and 7.3).

a. Major oxide:

Plot (Fig. 7.20A) reveals that:

1. Enrichment in Fe, Na, Ti and Mn and depletion in Mg, K in QPCs with respect to sandstones,
2. Little changes and closely constant proportion in Si, Al, Ca, and P in QPCs with respect to sandstones,
3. Strong and irregular variation in Fe and K in QPC with respect to sandstone.

b. Trace element:

Keonjhar Quartzite normalized QPC compositions of trace elements reveal (Fig.7.20B)

1. Enrichment in Cr, Ni, Th, U, Sr and Pb in QPCs with respect to the sandstone,
2. Depletion in Co, Rb, Cs and Ba in QPC samples with respect to the sandstone,
3. Comparable proportion in Cu, Zn, Ga, Y, Zr, Nb and Hf with respect to the sandstone.

c. Rare Earth Elements

REE compositions of the QPCs normalized to sandstones reveal (Fig. 7.20C)

1. Enrichment in LREE in QPC samples with respect to the sandstone
2. Elevated Eu content with respect to sandstone and retention of negative Eu anomaly in QPC samples with respect to rest of the REE even after normalization wrt sandstone.
3. Comparable HREE proportion with respect to sandstone.

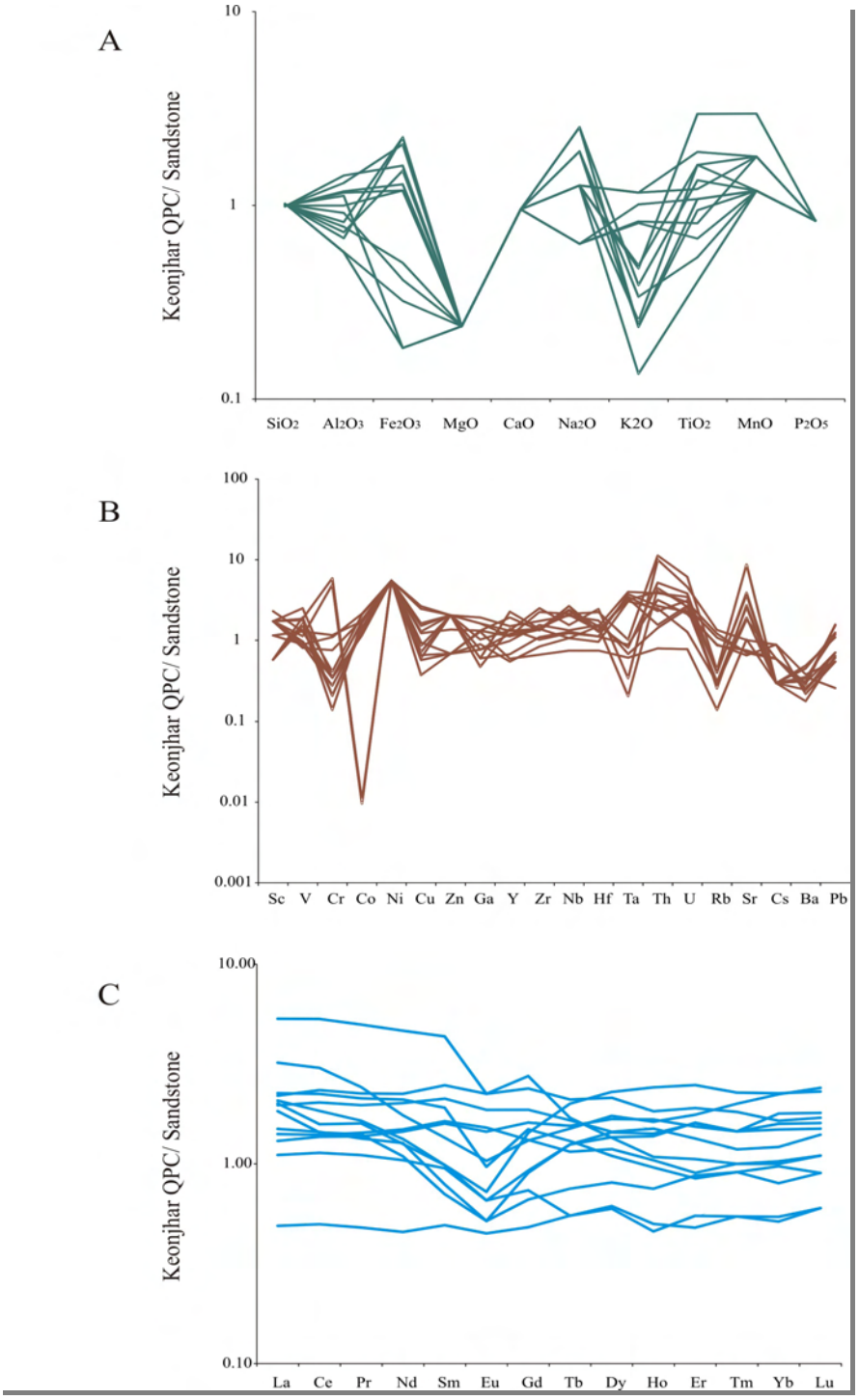

Fig. 7.20. Compositional plots of Keonjhar QPC normalized to host sandstones A. Major oxide variations normalized with respect to sandstones. Note: variable enrichment in Fe2O3, Na2O, TiO2 and MnO and depletion in MgO, K2O and P2O5. B. Trace element compositions normalized with respect to sandstone. Note enrichment in Cr, Ni, Th, U, Sr and Pb in QPC and depletion in Co, Rb, Cs and Ba. C. Rare Earth Element plot normalized with respect to sandstone. Note enrichment in LREE in QPC and retention of negative Eu-anomaly.

7.3.3.2. Chondrite normalized REE plot

Keonjhar QPCs here are again plotted against carbonaceous chondrites (McDonough and Sun 1995). (Fig. 7.21)

1. enrichment in LREE in Keonjhar QPC samples with respect to the chondrite
2. *negative Eu-anomaly* in Keonjhar QPC samples with respect to the chondrite
3. *flat HREE composition* in Keonjhar QPC samples with respect to the chondrite.

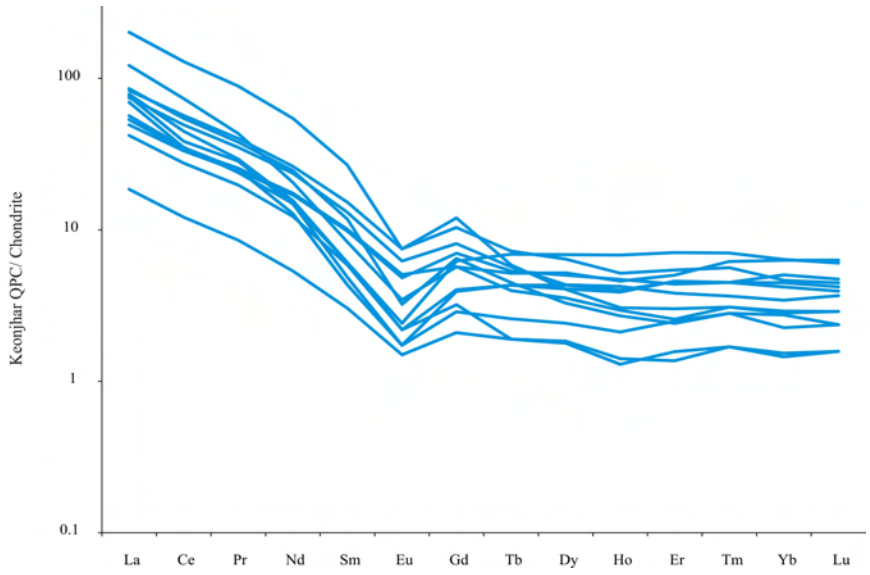

Fig. 7.21. Keonjhar QPC Rare Earth Element (REE)normalized diagram with respect to chondrite. Note considerable enrichment in the LREE and a consistent negative Eu-anomaly.

7.3.3.3. QPC composition normalized to Singhbhum Granite

When normalized with respect to Singhbhum Granite (composition after Saha 1994; Dey et al. 2017) the QPC reveals enrichment in Si, Al, Mn, K, Cu, Ga, Ni, Rb, V, Ta and LREE and depletion in Ca, Na, Cr, Pb, Sr, Y, with respect to the basement granitoids and little changes in Yb, Tb, Sm, Ce, Eu and Nd. Enrichment in Si, K, Rb

and LREE are common changes from granitic basement to shelf sandstones of all ages as ascribed commonly due to the effect of weathering (Fig. 7.22, Fig. 7.23 , Fig. 7.24 and Fig. 7.25).

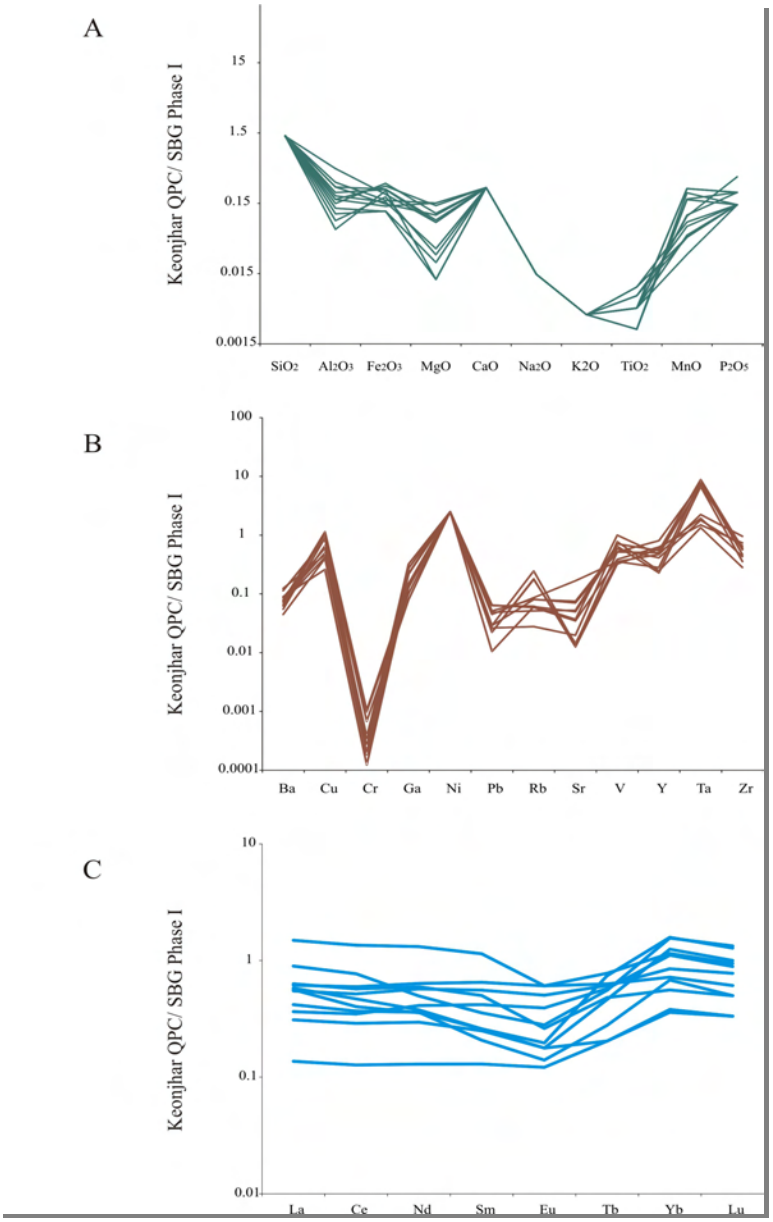

Fig.7.22. Compositional plots of Keonjhar QPC normalized to Singhbhum Granite Phase I A. Major oxide variations normalized with respect to Singhbhum Granite Phase I. Note. Enrichment of SiO2, Al2O3 and MnO. B. Trace element variations normalized with respect to Singhbhum Granite Phase I. Note enrichment of Cu, Ni, Rb, V and Ta. C. Rare Earth Element variations normalized with respect to Singhbhum Granite Phase I. Note. similar trend for LREE and HREE.

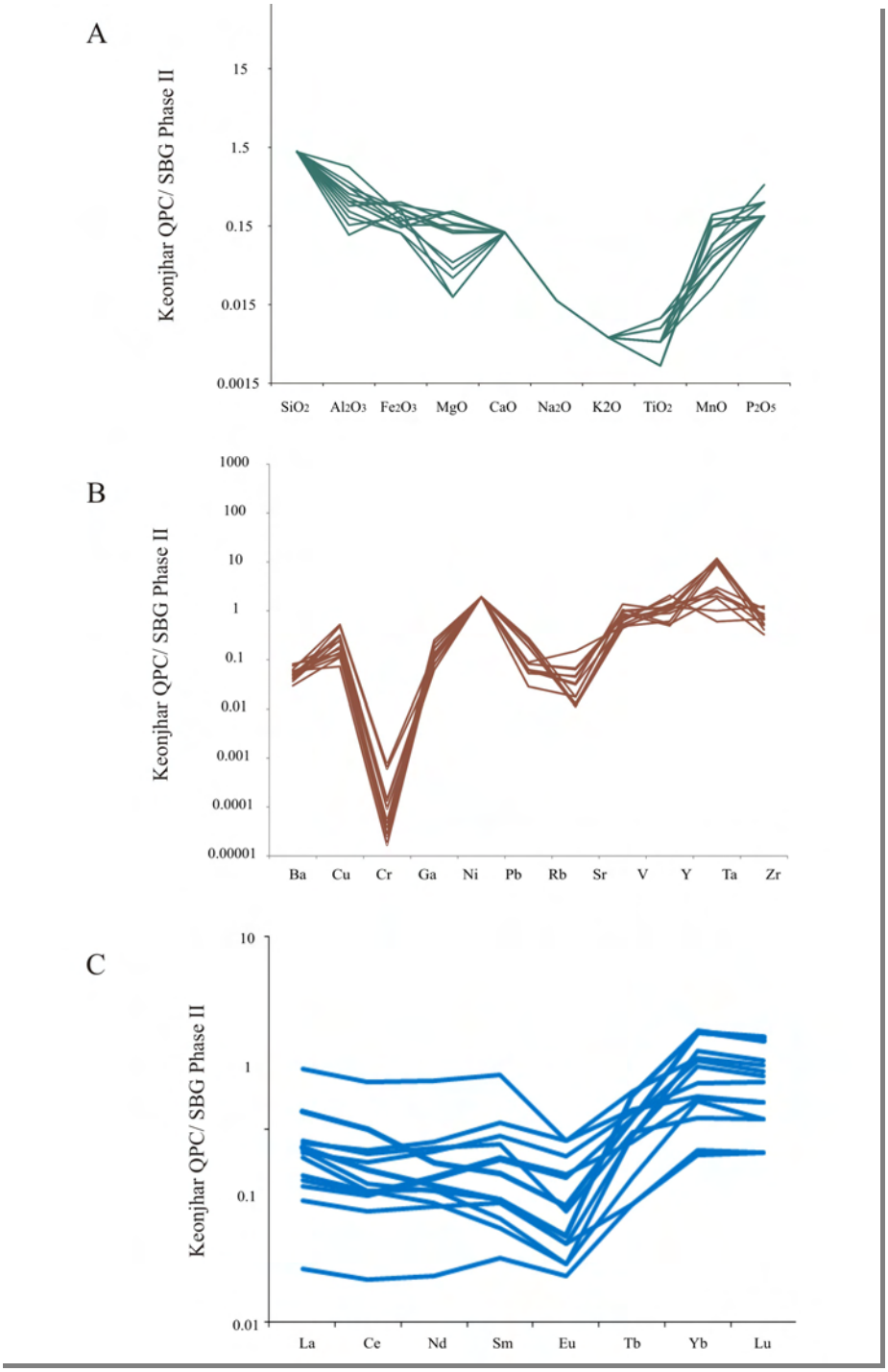

Fig.7.23. Compositional plots of Keonjhar QPC normalized to Singhbhum Granite Phase II A. Major oxide variations normalized with respect to Singhbhum Granite Phase II. Note enrichment of SiO2, Al2O3 and MnO. B. Trace element variations normalized with respect to Singhbhum Granite Phase II. Note enrichment of Cu, Ni, V and Ta. C. Rare Earth Element variations normalized with respect to Singhbhum Granite Phase II. Note negative Eu- anomaly and enrichment of HREE.

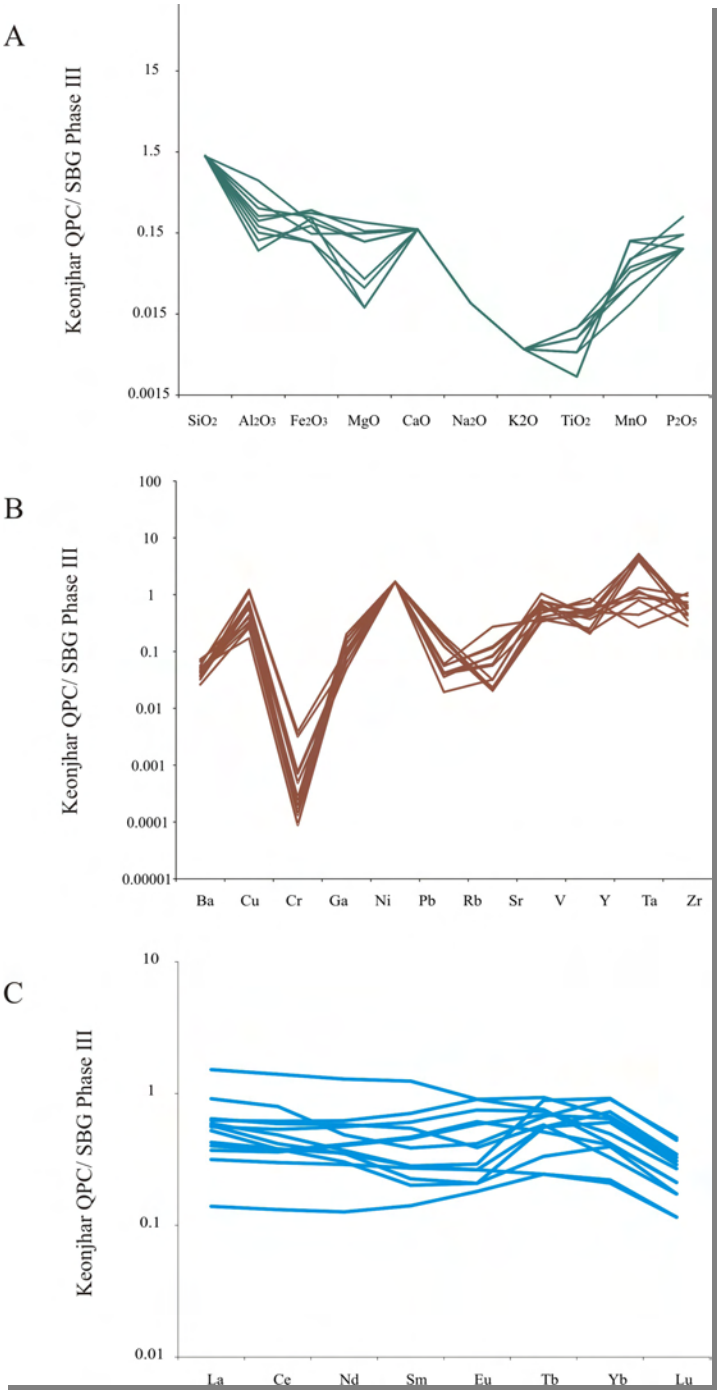

Fig.7.24. Compositional plots of Keonjhar QPC normalized to Singhbhum Granite Phase III A. Major oxide variations normalized with respect to Singhbhum Granite Phase III. Note enrichment of SiO2, Al2O3 and MnO. B. Trace element variations normalized with respect to Singhbhum Granite Phase III. Note enrichment of Cu, Ni and V. C. Rare Earth Element variations normalized with respect to Singhbhum Granite Phase III. Note flat trend for LREEs and HREEs.

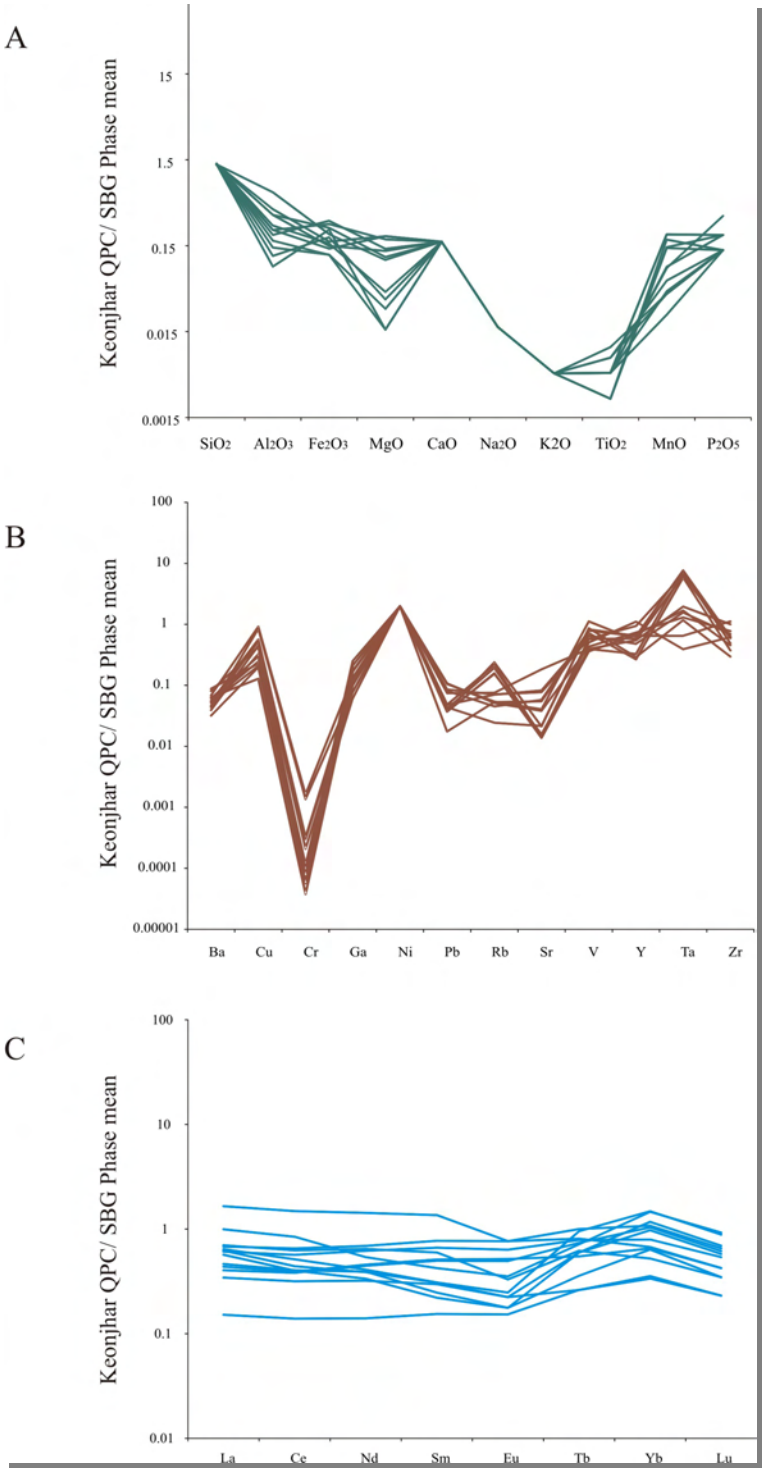

Fig.7.25. Compositional plots of Keonjhar QPC normalized to Singhbhum Granite all Phase (mean value) A. Major oxide variations normalized with respect to Singhbhum Granite Phase mean. Note enrichment of SiO2, Al2O3 and MnO. B. Trace element variations normalized with respect to Singhbhum Granite Phase mean. Note enrichment of Cu, Ni and V. C. Rare Earth Element variations normalized with respect to Singhbhum Granite Phase mean. Note flat trend for LREEs and HREEs.

7.3.4. Correlation of U-Th with respect to other elements

To explore further relationship between concentrations of U, Th with respect to other elements, correlation matrix has been calculated (Table 7.4, 7.5, 7.6 and 7.7, Fig. 7.26) and the salient observations are summarized below:

a. U, Th vs major oxides (Fig. 7.26A)

1. positive correlation with Th, MnO and TiO_2 within QPC samples
2. negative correlation with SiO_2, Al_2O_3 and Na_2O within QPC samples
3. slightly negative correlation with Fe_2O_3 and K_2O

b. U, Th vs trace elements (Fig. 7.26B)

1. positive correlation with Zr, Ti, Hf , Th, Sr and Ba within QPC samples
2. negative correlation with V, Co and Ta within QPC samples
3. Low negative correlation with Sc, Cr, Cu, Ga, Y, Nb, Rb and Pb within QPC samples.

c. U, Th vs LREE (Fig. 7.26C)

1. Generally positive correlation with Th and LREE within QPC samples

d. U, Th-HREE (Fig. 7.26D)

1. low positive correlation with Th and Gd within QPCs
2. low negative correlation with Tb, Dy, Ho, Er, Tm, Yb and Lu within QPCs

7.4. Discussion

7.4.1. Uranium mineralogy

Detrital uraninite content in Precambrian rocks is considered as evidence for oxygen deficient atmosphere. The Keonjhar QPC surface samples studied here do not reveal the presence of detrital uraninite. However, the presence of uraniferous leucoxene or rutile, brannerite, coffinite, thorite, uranothorite from Keonjhar QPCs suggests potential radioactive mineralization in the QPCs. Brannerite is most common

uranium containing mineral in this QPC. Brannerite is generally associated with uraninite within conglomerate matrix. These types of deposits are commonly found in Elliot lakes-Blind River area in Ontario, Canada and Witwatersrand basin in South Africa (Saager and Stupp 1983). Brannerite is predominant U-bearing mineral in the Keonjhar QPC surface samples. Brannerite formation is mainly considered as diagenetic process when dissolved uranium from detrital uraninites or from *paleosols* underlying brannerite-bearing QPCs reacts with rutile in QPCs. Ramdohr (1957) suggested that brannerite forms in the basal siliciclastics overlyng '*Pronto Paleosol'* through such diagenetic reaction and the reaction is coined as the *Pronto Reaction*.

$$UO_2 + 2\text{-}3\ TiO_2 \longrightarrow UTi_{2\text{-}3}O_{6\text{-}8}$$

When uranium migrates into Ti phases or titanium migrates into uranium phases the replacement reactions give rise to a spectrum of U-Ti oxide phases such as brannerite/leucoxene/uranium rutile/uranium free rutile. Mukhopadhyay et al. (2016) already documented QPC hosted uraninite placer mineralization from Mahagiri Quartzite. Mukhoadhyay et al. (2014) based on detrital zircon (< 3Ga, U-Pb) correlated Mahagiri Quartzite with the Keonjhar Quartzite studied here. U-Ti-bearing minerals in the presently studied QPCs might indicate uraninite-bearing strata in subsurface below the present day weathering profile. The presence of zoned grains with U-rich brannerite rim overgrown around Ti-rich core (Fig. 7.6) provides evidence for diagenetic origin of brannerite in the Keonjhar QPC. The geological setting of the Keonjhar Quartzite with Keonjhar Paleosol underneath along the unconformity is closely comparable with the brannerite bearing QPCs of the Elliot Lake deposits overlying the Pronto Paleosol. Rare occurences of euhedral coffinite in the Keonjhar QPC points to diagenetic U-mineralization in a reducing condition.

7.4.2. Nature of the upper crust as a potential source of U-Th paleoplacers

Cr/Th versus Sc/Th (Fig. 7.15, fields after Condie and Wronkiewicz 1990) and Cr/V versus Y/Ni (Fig. 7.16A) and other trace elemental ratios such as Th/Sc, La/Sc and La/Th (fields after Taylor and McLennan 1985; Cullers et al. 1988; McLennan and Taylor 1991; Cullers 1994; Armstrong-Altrin et al. 2004; Yan et al. 2012) reveal that these sediments are of passive margin as well as active margin affinity (cf. Ghosh et al. 2016). This mixed source origin reveals both cratonic and recycled orogen provenance types. Archean sediments are generally enriched in Cr, Sc, Ni and depleted in Th, Y (cf. Ghosh et al. 2016). High Cr/Th and Sc/Th ratio in some samples indicate a mafic source origin. The more felsic origin favors source of sediments from differentiated crust with minor mafic components influences that could have come from active tectonic setting. The wide variation in Y/Ni ratio in the Keonjhar sample reflects derivation from multiple provenance. Similarly, Th/Sc wide variation supports multicomponent source. QPC and mature quartz arenite show high Zr/Sc range typical of zircon accumulation presumably associated with sediment recycling and sorting. The negative Eu-anomalies in Keonjhar QPC and arenites suggests the existence of evolved and differentiated granitoid components in the upper crust. The intracratonic tectonic setting of the depositional system indicates Mesoarchean stabilization of the Singhbhum craton (cf. Ghosh et al. 2016). The differentiated crust and passive margin cratonic setting for the source terrane therefore, suggest positive enrichment of U-Th minerals in the late phase crustal differentiates in the Singhbhum granitoid upper crust.

7.4.3. Granitic basement to siliciclastic depositional sink

Basement-cover compositional variation is an important tool for understanding the transfer of elements from continental crust to the marine sink. Additionally for sediments older than GOE the redox state of atmosphere can also play an important role in such processes. The variations from source to sink recorded in such sediments are likely to be controlled by factors such as weathering condition, role of biomediation in release and retention of elements. Enrichment of Al, and Ga in Keonjhar Quartzite indicates the role of recycled sediment source in enrichment of immobile elements (Ghosh et al. 2016). K enrichment over Na implies illitization during diagenesis. Several proxies such as Ta and LREE and compatible elements (V, Ni) enrichment in the sandstone and QPC, point to mixed source terrain. Felsic components are likely to be the source of differentiated crust, whereas mafic component influenced by volcanic, active tectonic source presumably sourced from greenstone enclaves within the basement granitoids. Detrital sulphide population in the quartzite points to pre-GOE sediment transport from land to the sea. Higher concentration of Zr and Ta in QPC and sandstone with respect to the granitic basement possibly indicate sediment recycling during transport. Abundance of Yb, Tb, Sm and Ce and depletion of Eu, Nd in the depositional sink are likely to be controlled by the detrital zircons. LREE enrichment and positive Ce anomaly may indicate the presence of monazite and other U-Th phosphate phases in the QPCs that are likely to be products of supergene alteration of detrital U-Th phases in the QPCs.

7.4.4. Difference between QPCs and quartzite of Keonjhar region

A comparative study of compositions between QPC and quartzites reveals relative enrichment in Fe, Na, Ti, Cr, Ni, Th, U, Sr, Pb, depletion in Mg, K, Co, Rb, Cs and

Ba in the former and very little change in of Si, Al, Ca, P, Cu. Enrichment of Fe and Cr in QPC over Keonjhar sandstone may suggest enrichment detrital redox sulphide phases in QPCs. Ni-enrichment in QPCs compared to sandstone also suggests enrichment of detrital sulphide minerals. Elements such as Cu, Fe, Mn and Ni are indicating enrichment detrital sulphides in the Keonjhar alluvial sediments. Enrichment of LREE in the QPCs relative to sandstones could be due to deposition of phosphate minerals in the supergene alteration stage. Complex microcrystalline aggregate of U-bearing supergene phosphates are likely to be the sink of the LREEs.

7.4.5. Implications for QPC-hosted Uranium mineralization

The geochemical and petrographic (including SEM) studies reveal that the radioactive mineralization of Mesoarchean Keonjhar QPC is composed of rutile/ uraniferous leucoxene aggregate associated with coffinite, thorite, uranothorite, zircon, pyrite and monazite. Detail study of the Mesoarchean Keonjhar QPC reveals that rutile/leucoxene and uranium enriched brannerites are predominant mineral over all other uraniferous phase. U-Ti phases are restricted within QPC just above the unconformity. From external morphology, geochemical composition and core-rim structure, brannerite and all U-Ti phases speak in favour of diagenetic alternations. Correlations of concentration of U and Th wrt other elements reveal positive correlation with TiO_2, Zr, and Hf. Correlations with Ti, Zr and Hf in turn suggest that uranium concentration is related to the concentration of detrital rutile and hence detrital zircon. A low positive or no correlation of U with redox sensitive elements (V, Cr, and Cu) may indicate that U- here is not associated with redox sulphides common to detrital uraninite redox placers. U also reveals positive correlation with LREEs indicating preferential U-concentration in supergene phosphate phases. The elemental

correlations of U and other elements is likely to suggest that the U-concentration in QPCs took place in the supergene weathering profile through alteration of Ti-bearing phases (Pronto Reaction). Such signature may be important in understanding hidden redox U-paleoplacers below the supergene weathering profile.

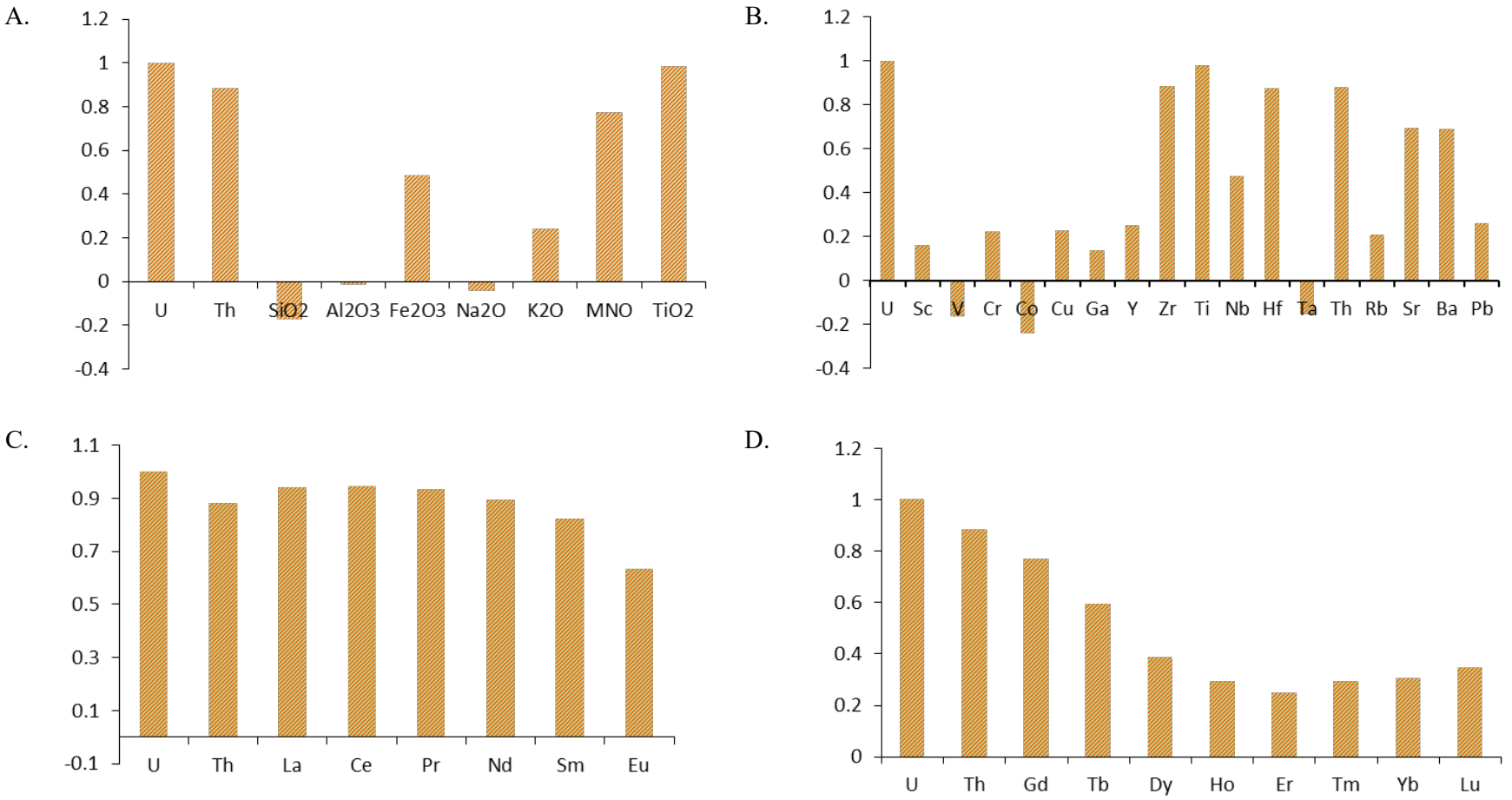

Fig. 7.26. Histogram showing the correlation coefficient from the correlation matrix for compositions of U, Th with respect to A. Major oxides B. Trace elements. C. LREE D. HREE.

Table 7.1. Major oxide composition (in wt %) of sandstone, mudstone, shale and conglomerates (QPC).

Sample	SiO_2	Al_2O_3	Fe_2O_3	MgO	CaO	Na_2O	K_2O	TiO_2	MnO	P_2O_5	LOI	Total
Sandstone												
KNJ-61B	93.29	4.07	0.25	0.08	<0.01	0.01	1.17	0.07	0.03	<0.01	0.8	99.77
KNJ-61D	92.46	4.16	0.46	0.09	<0.01	0.01	1.17	0.45	0.02	<0.01	0.9	99.72
KNJ-70B	93.16	5.05	<0.04	<0.01	<0.01	0.02	0.14	0.07	0.01	<0.01	1.3	99.75
KNJ-67F	97.99	0.92	<0.04	<0.01	<0.01	<0.01	0.26	0.02	0.01	<0.01	0.5	99.7
KNJ-67G	97.58	1.37	<0.04	<0.01	<0.01	<0.01	0.37	0.03	0.02	<0.01	0.4	99.77
KNJ-67E	98.2	0.92	<0.04	<0.01	<0.01	<0.01	0.25	0.02	0.02	<0.01	0.4	99.81
KNJ-64J	96.97	1.97	<0.04	<0.01	<0.01	<0.01	0.14	0.04	0.01	<0.01	0.6	99.73
KNJ-64I	95.24	3.46	<0.04	<0.01	<0.01	<0.01	0.05	0.03	0.02	<0.01	1	99.8
KNJ-64H	95.64	3.15	0.04	<0.01	<0.01	<0.01	0.04	0.03	0.02	<0.01	0.9	99.82
KNJ-64G	96.53	2.41	<0.04	<0.01	<0.01	<0.01	0.1	0.03	0.03	<0.01	0.7	99.8
KNJ-64F	96.01	2.84	0.05	<0.01	<0.01	<0.01	0.14	0.05	0.01	<0.01	0.6	99.7
KNJ-64C/1	95.91	2.68	0.52	0.01	<0.01	0.05	0.24	0.02	0.03	<0.01	0.5	99.96
KNJ-64E	95.85	2.95	<0.04	<0.01	<0.01	0.02	0.09	0.03	0.01	<0.01	0.8	99.75
KNJ-61A	93.79	3.62	0.53	0.09	0.02	0.01	1.05	0.06	0.02	<0.01	0.7	99.89
KNJ-67H	97.79	1.1	0.51	<0.01	<0.01	<0.01	0.3	0.03	0.02	<0.01	0.2	99.95
KNJ-48A	92.76	4.21	0.37	0.1	0.01	0.02	1.31	0.06	<0.01	0.02	1	99.86
KNJ-48J	94	3.62	0.24	0.1	0.01	0.02	1.15	0.11	0.01	0.02	0.4	99.68
KNJ-49A	90.32	5.68	0.39	0.11	0.01	0.03	1.65	0.14	0.01	0.02	1.4	99.76
KNJ-49B	90.3	5.67	0.46	0.11	0.01	0.02	1.65	0.12	<0.01	0.02	1.5	99.86
KNJ-48A	92.76	4.21	0.37	0.1	0.01	0.02	1.31	0.06	0.01	0.02	0.65	99.52
KNJ-48J	94	3.62	0.24	0.1	0.01	0.02	1.15	0.11	0.01	0.02	0.1	99.38
KNJ-49A	90.32	5.68	0.39	0.11	0.01	0.03	1.65	0.14	0.01	0.02	1.32	99.68
KNJ-49B	90.3	5.67	0.46	0.11	0.01	0.02	1.65	0.12	0.01	0.02	0.87	99.24
KNJ 46C	97.23	1	0.07	0.01	0.02	0.03	0.14	0.02	0.02	0.01	1.21	99.76
KNJ 45J	96.79	0.96	0.04	0.01	0.01	0.02	0.17	0.02	0.02	0.01	1.98	100.03
KNJ 45C	95.96	0.84	0.02	0.01	0.01	0.02	0.13	0.02	0.02	0.01	1.83	98.87
KNJ 45I	96.32	1.27	0.05	0.01	0.01	0.02	0.27	0.05	0.02	0.01	0.97	99
KNJ 45H	96.83	0.92	0.04	0.01	0.01	0.02	0.16	0.03	0.02	0.01	1.22	99.27

Table 7.1. Continuation…..

KNJ 45L	96.32	1.27	0.05	0.01	0.01	0.02	0.27	0.03	0.02	0.01	0.58	98.59
KNJ 46B	96.86	0.95	0.03	0.01	0.01	0.03	0.12	0.02	0.02	0.01	1.25	99.31
KNJ 45K	96.42	1.25	0.06	0.01	0.01	0.02	0.25	0.04	0.02	0.01	0.93	99.02
KNJ 46A	96.91	1.04	0.04	0.01	0.01	0.03	0.15	0.03	0.02	0.01	0.84	99.09
KNJ 48E	94.5	3.04	0.16	0.06	0.01	0.02	0.86	0.07	0.02	0.01	0.76	99.51
KNJ 48C	94.27	2.94	0.15	0.06	0.01	0.02	0.85	0.1	0.02	0.01	1.1	99.53
Mudstone												
KNJ-73B	52.28	15.28	16.05	8.1	0.03	<0.01	0.06	0.74	0.02	0.36	6.7	99.62
KNJ-73C	53.26	14.85	15.9	8.22	0.03	<0.01	0.02	0.72	0.02	0.37	6.3	99.69
KNJ-73D	52.51	15.15	16.04	8.17	0.03	<0.01	0.04	0.74	0.02	0.37	6.6	99.67
Shale												
KNJ-47D	89.26	7.78	0.12	0.01	0.01	0.04	0.07	0.18	<0.01	<0.01	2.5	99.97
KNJ-47H	93.97	4.05	0.1	0.01	0.01	0.05	0.06	0.05	<0.01	0.01	1.6	99.91
KNJ-47J	87.24	8.52	0.26	0.02	0.02	0.11	0.17	0.33	<0.01	0.02	3.1	99.79
QPC												
KNJ-73E	93.64	4.49	0.35	0.01	0.01	0.04	0.14	0.07	0.02	<0.01	1	99.77
KNJ-73F	94.14	3.66	0.26	0.01	<0.01	0.04	0.23	0.1	0.02	<0.01	1.2	99.66
KNJ-73G	93.83	4.11	0.45	<0.01	<0.01	0.03	0.14	0.08	0.02	<0.01	1	99.66
KNJ-64A	95.77	2.88	0.09	<0.01	<0.01	0.03	0.2	0.04	0.02	<0.01	0.7	99.73
KNJ-64B	95.01	3.53	<0.04	<0.01	<0.01	0.02	0.08	0.03	0.02	<0.01	1.1	99.79
KNJ-64C	96.03	2.29	0.33	<0.01	<0.01	0.02	0.29	0.12	0.03	<0.01	0.6	99.71
KNJ-64D	94.79	3.14	0.26	<0.01	0.01	0.02	0.28	0.22	0.05	<0.01	0.9	99.67
KNJ-67J	96.82	1.8	0.04	<0.01	<0.01	0.01	0.49	0.06	0.03	<0.01	0.4	99.65
KNJ-67I	96.76	1.81	0.07	<0.01	<0.01	<0.01	0.48	0.05	0.02	<0.01	0.4	99.59
KNJ-67C	95.7	2.44	0.11	<0.01	<0.01	0.02	0.69	0.09	0.03	<0.01	0.6	99.68
KNJ-70A	94.18	3.72	0.28	<0.01	<0.01	0.02	0.15	0.12	0.02	<0.01	1.1	99.59
KNJ-67A	96.16	2.13	0.49	<0.01	<0.01	0.01	0.6	0.08	0.02	<0.01	0.4	99.89
KNJ-67D	95.41	2.58	0.49	<0.01	<0.01	0.02	0.69	0.14	0.03	<0.01	0.5	99.86

Table 7.2. Trace element concentration (in ppm) of sandstone, mudstone, shale and conglomerates (QPC).

Sample	Sc	V	Cr	Co	Ni	Cu	Zn	Ga	Y	Zr	Nb	Hf	Ta	Th	U	Rb	Sr	Cs	Ba	Pb
Sandstone																				
KNJ-61B	2	16	0.00479	137.4	2.8	1.6	2	3.7	11.9	69	1.7	2.1	0.7	3.1	2.1	40.9	3.3	0.5	162	4.3
KNJ-61D	4	20	0.02668	167	4.8	11	2	3.9	13.3	165.2	6.7	4.4	3.5	8.5	3.9	38.9	4.1	0.7	158	18.6
KNJ-70B	2	11	0.00274	216.2	4	2.1	<1	3.8	6.9	68.8	3.2	1.9	3.8	4.4	1.9	5.2	7.7	<0.1	22	2
KNJ-67F	1	<8	0.00137	274.5	4.1	2	<1	<0.5	2.2	46.1	1.5	1.2	4.4	1.6	0.6	8.3	1.3	<0.1	8	0.6
KNJ-67G	1	13	0.00137	185.4	2.5	2.2	<1	<0.5	3.5	85.4	1.1	2.3	0.9	4.2	1.5	13.3	3.3	<0.1	10	0.6
KNJ-67E	1	<8	0.00137	193.7	2.6	1.7	<1	<0.5	2.6	52.7	0.9	1.4	0.8	2.4	0.9	8.5	1.8	<0.1	6	0.7
KNJ-64J	1	<8	0.00137	172.2	2.7	3.1	2	0.9	4.8	56.6	1	1.6	0.8	2.1	0.6	3.1	11.1	<0.1	22	1.4
KNJ-64I	1	8	0.00137	111.1	1.5	2.4	<1	2.2	4.3	51.4	1.2	1.4	2.2	2.2	0.6	1.3	7.7	<0.1	7	0.9
KNJ-64H	<1	9	0.00137	118.6	1.7	1.9	<1	1.7	3.2	45.9	0.6	1.2	0.5	1.9	0.4	0.8	6.7	<0.1	4	0.9
KNJ-64G	<1	9	0.00137	143.7	3	2.3	<1	0.8	4.4	49	1	1.4	0.8	2.4	0.7	2.5	8.2	<0.1	12	1.1
KNJ-64F	2	10	0.00137	249	3.3	1.9	<1	1.3	3.9	58.4	2.1	1.4	4	4	0.7	3.8	9.2	<0.1	13	1.2
KNJ-64C/1	<1	10	0.04446	1.3	7.4	12.4	1	1	4	54.2	0.5	1.6	0.1	2.6	1	6.4	7.5	<0.1	13	1.1
KNJ-64E	1	12	0.00137	164.6	2.7	0.9	<1	1.8	3.5	43.3	0.9	1.2	0.7	2.5	1.1	2.5	6.5	<0.1	32	0.8
KNJ-61A	2	15	0.03762	0.9	5.7	4.2	3	3.1	10.5	63.1	1.2	1.9	0.2	2.7	1.8	38.2	3.9	0.8	140	4.1
KNJ-67H	<1	9	0.04378	0.8	7.4	5.7	1	<0.5	3.4	73.1	0.8	1.9	<0.1	3.1	1.3	10.4	3.5	0.1	7	0.6
KNJ-48A	2	13	0.003	140.8	3.1	2.0	2	4.6	7.9	66.1	2.5	1.9	0.3	3.0	0.7	44.8	8.0	0.5	186	4.2
KNJ-48J	3	17	0.008	224.3	3.4	1.9	1	3.2	7.0	99.3	3.8	2.5	3.8	2.1	1.9	40.9	8.4	0.7	184	4.8
KNJ-49A	3	21	0.008	158.5	3.7	4.3	3	5.1	12.5	81.3	2.9	2.4	0.5	2.2	2.9	52.8	7.2	1.0	222	6.9
KNJ-49B	3	19	0.008	109.9	2.7	3.0	2	5.6	12.1	79.2	2.2	2.0	0.2	2.5	2.4	52.8	7.4	1.0	199	4.6
Mudstone																				
KNJ-73B	33	253	0.04925	60.7	224	8.4	154	20.7	25.2	143.2	7.3	3.8	0.5	4.7	3.1	3.1	17.2	0.3	28	3.5
KNJ-73C	32	239	0.04925	60.6	215	3.6	150	21	27.8	142.4	7.2	3.8	0.6	4.9	3.2	1.7	10.8	0.1	27	2.6
KNJ-73D	33	245	0.04925	56.7	221	3.6	156	19.9	25	142.4	6.9	4	0.6	4.6	2.9	2.3	15.1	0.2	28	2.8
Shale																				
KNJ-47D	4	47	0.013	34.5	<20	12.7	<1	6.9	8.4	37.4	4.1	0.8	1.1	2.6	1.4	2.1	10.6	<0.1	15	0.3

Table 7.2 Continuation…..

KNJ-47H	2	29	0.005	56.4	<20	1.4	<1	4.0	1.8	26.4	1.3	0.7	0.2	1.2	0.3	1.7	6.8	<0.1	13	0.3
KNJ-47J	6	54	0.025	84.4	<20	5.6	<1	8.8	17.0	177.1	7.7	4.4	0.8	7.7	2.6	5.7	33.1	<0.1	38	0.6
QPC																				
KNJ-73E	3	12	0.00342	167.7	<20	2.1	3	4.5	9.6	119.2	3.8	3.3	1	4.3	3.5	5.7	11.1	0.2	21	4.9
KNJ-73F	2	16	0.00342	251.4	<20	4.3	2	3.1	12.3	91.3	4.4	2.4	5.1	7	4.4	7.9	22.5	0.1	33	3.9
KNJ-73G	3	31	0.00342	249.1	<20	2.5	3	3.8	7.2	93.3	5	2.4	4.9	4.7	3.8	6	11.8	<0.1	23	4.8
KNJ-64A	1	20	0.001368	241.2	<20	1.3	<1	2.1	3.5	57.5	2	1.8	4.5	7.5	1.8	5.9	15.9	<0.1	26	0.8
KNJ-64B	1	24	0.002052	191.6	<20	2	<1	3	3.8	45.6	1.4	1.4	0.9	2.4	1.1	2.7	6.3	<0.1	13	2
KNJ-64C	1	18	0.002052	208.1	<20	3.3	<1	1.8	6.3	106.5	2.5	2.9	1.2	15.7	5.4	7.8	24	<0.1	18	2.2
KNJ-64D	2	11	0.002736	194.6	<20	2.3	1	3.1	7.2	154.5	4	4.2	1.5	34.1	8.7	8.4	53.4	<0.1	36	3.4
KNJ-67J	3	10	0.007524	261.3	<20	4.5	3	1.1	8.9	70	2.3	2.1	1.3	9.6	3	17.5	4	0.3	16	1.7
KNJ-67I	3	11	0.010944	311.1	<20	5.3	3	1.4	4.3	75.2	2.4	2.1	5.5	8.1	3.2	17.1	4.6	0.2	19	1.7
KNJ-67C	4	16	0.011628	250.1	<20	5.7	3	1.8	7.7	98.4	3.9	2.5	4.7	12.1	4.2	23.9	4.3	0.2	22	2.2
KNJ-70A	3	22	0.004104	303	<20	3	3	3.8	8.4	96	4.5	2.8	5.9	11.6	4.9	5	16.8	<0.1	25	3.7
KNJ-67A	3	14	0.049248	1.4	<20	8.6	3	1.4	14.5	95.1	2	2.8	0.3	13.4	3.7	21.4	4.4	0.2	18	1.9
KNJ-67D	3	23	0.058824	1.5	<20	9.3	3	2.4	8.5	172.1	2.9	4.6	0.5	30.3	6.5	26.5	6.2	0.3	28	1.7

Table 7.3. Rare Earth Element concentration (in ppm) of sandstone, mudstone, shale and conglomerates (QPC).

Sample	La	Ce	Pr	Nd	Sm	Eu	Gd	Tb	Dy	Ho	Er	Tm	Yb	Lu	Total REE
Sandstone															
KNJ-61B	16.2	31.9	3.36	12.2	2.29	0.45	2.08	0.32	1.85	0.39	1.15	0.17	1.1	0.16	73.62
KNJ-61D	25.8	40.6	4.57	16.3	2.92	0.62	2.78	0.42	2.41	0.5	1.47	0.23	1.34	0.2	100.16
KNJ-70B	14	23.8	2.47	8.9	1.75	0.3	1.72	0.25	1.42	0.29	0.81	0.11	0.74	0.11	56.67
KNJ-67F	3.8	6.8	0.67	2.3	0.5	0.09	0.53	0.08	0.43	0.1	0.31	0.04	0.34	0.05	16.04
KNJ-67G	23.5	32.7	2.85	7.7	0.83	0.13	0.76	0.12	0.74	0.16	0.6	0.1	0.73	0.1	71.02
KNJ-67E	9.2	14.2	1.31	3.9	0.46	0.12	0.47	0.09	0.56	0.11	0.38	0.05	0.41	0.06	31.32
KNJ-64J	10.4	17.4	1.87	6.6	1.34	0.29	1.04	0.16	0.92	0.19	0.55	0.08	0.51	0.08	41.43
KNJ-64I	8.4	14.1	1.53	5.3	0.83	0.23	0.8	0.13	0.72	0.15	0.46	0.06	0.45	0.07	33.23
KNJ-64H	7.2	12.2	1.33	4.4	0.84	0.2	0.67	0.1	0.53	0.11	0.38	0.06	0.35	0.05	28.42
KNJ-64G	8.3	14	1.5	5.4	0.9	0.17	0.8	0.12	0.64	0.14	0.47	0.07	0.35	0.06	32.92
KNJ-64F	10.6	16.7	1.77	6.3	1.03	0.25	0.87	0.11	0.57	0.15	0.42	0.06	0.42	0.06	39.31
KNJ-64C/1	11.5	21.4	2.26	8.1	1.24	0.27	1.04	0.13	0.75	0.14	0.41	0.06	0.45	0.06	47.81
KNJ-64E	6.9	12	1.27	4.5	0.64	0.16	0.76	0.12	0.65	0.12	0.38	0.05	0.37	0.06	27.98
KNJ-61A	20.5	41.4	4.47	15.2	2.65	0.59	2.49	0.34	1.72	0.35	0.99	0.17	0.99	0.14	92
KNJ-67H	20.1	31.1	2.86	8.3	0.93	0.16	0.88	0.13	0.71	0.16	0.55	0.09	0.54	0.09	66.6
KNJ-48A	10.3	17.1	2.05	7.7	1.39	0.33	1.34	0.21	1.26	0.27	0.78	0.11	0.75	0.12	43.71
KNJ-48J	20.1	33.4	3.62	12.3	2.12	0.44	2.12	0.27	1.44	0.27	0.77	0.14	0.85	0.14	77.98
KNJ-49A	18.8	30.4	3.29	11.7	2.07	0.30	1.99	0.38	2.18	0.51	1.38	0.22	1.42	0.18	74.82
KNJ-49B	18.5	30.7	3.34	11.4	2.22	0.40	2.22	0.37	2.20	0.46	1.26	0.20	1.26	0.17	74.7
Mudstone															
KNJ-73B	19.7	41.9	4.88	19.5	4.34	2.08	4.45	0.68	4.16	0.9	2.82	0.39	2.56	0.39	108.75
KNJ-73C	11.3	23.9	2.85	11	2.91	1.87	4.37	0.76	4.57	0.95	3.01	0.39	2.6	0.41	70.89
KNJ-73D	16.8	36.4	4.14	17	3.94	2.03	4.4	0.7	4.28	0.92	2.8	0.4	2.48	0.4	96.69
Shale															
KNJ-47D	19.6	30.6	3.43	11.7	1.93	0.35	1.88	0.30	1.63	0.28	0.81	0.13	0.77	0.12	73.53
KNJ-47H	4.8	6.9	0.75	2.6	0.42	0.09	0.39	0.06	0.41	0.10	0.25	0.04	0.27	0.03	17.11
KNJ-47J	35.0	58.6	6.86	24.4	4.65	0.82	4.16	0.62	3.35	0.63	1.71	0.28	1.90	0.28	143.26
QPC															
KNJ-73E	18.1	31.8	3.35	12.1	2.26	0.42	2.14	0.31	1.91	0.4	1.09	0.16	1.11	0.16	75.31
KNJ-73F	30.5	54.4	5.49	18.7	3.51	0.65	3.17	0.42	2.44	0.44	1.35	0.2	1.15	0.17	122.59

Table 7.3. Continuation…..

KNJ-73G	19.6	32.5	3.49	12.4	2.32	0.44	1.75	0.23	1.35	0.25	0.64	0.11	0.7	0.11	75.89
KNJ-64A	15.4	26.4	2.7	8.7	1.35	0.19	0.98	0.11	0.68	0.11	0.39	0.06	0.38	0.06	57.51
KNJ-64B	6.8	11.6	1.17	3.8	0.7	0.13	0.64	0.11	0.7	0.12	0.34	0.06	0.36	0.06	26.59
KNJ-64C	31.4	52.1	5.19	17.5	2.71	0.28	1.98	0.26	1.25	0.23	0.6	0.1	0.56	0.09	114.25
KNJ-64D	74.1	123.6	12.16	38.7	6.17	0.65	3.66	0.34	1.54	0.26	0.75	0.11	0.72	0.11	262.87
KNJ-67J	25.5	33.4	3.43	9.1	1	0.15	1.2	0.25	1.64	0.34	1.13	0.16	1.04	0.15	78.49
KNJ-67I	20.8	33.6	3.27	10.6	1.12	0.15	0.88	0.15	0.92	0.18	0.62	0.1	0.68	0.09	73.16
KNJ-67C	27.9	36.7	3.89	10.5	1.4	0.19	1.23	0.25	1.55	0.33	1.14	0.16	1.25	0.18	86.67
KNJ-70A	27.3	47.2	4.8	16.8	3.01	0.54	2.48	0.33	1.65	0.36	0.95	0.13	0.85	0.14	106.54
KNJ-67A	28.8	42.8	4.01	11.1	1.4	0.21	1.9	0.4	2.61	0.58	1.76	0.25	1.58	0.23	97.63
KNJ-67D	44.6	70.3	5.91	14.6	1.92	0.3	1.74	0.3	1.98	0.39	1.25	0.22	1.56	0.24	145.31

Table 7.4. Correlation matrix of major elements with U and Th

	U	**Th**	**SiO_2**	**Al_2O_3**	**Fe_2O_3**	**Na_2O**	**K_2O**	**MnO**	**TiO_2**
U	1								
Th	0.883	1							
SiO_2	-0.173	0.129	1						
Al_2O_3	-0.016	-0.281	-0.972	1					
Fe_2O_3	0.484	0.355	-0.401	0.274	1				
Na_2O	-0.042	-0.286	-0.789	0.808	0.2	1			
K_2O	0.239	0.44	0.638	-0.75	0.105	-0.571	1		
MNO	0.775	0.825	0.14	-0.242	-0.003	-0.245	0.26	1	
TiO_2	0.982	0.873	-0.236	0.058	0.437	-0.011	0.13	0.8	1

Table 7.5. Correlation matrix of trace elements with U and Th

	U	Sc	V	Cr	Co	Cu	Ga	Y	Zr	Ti	Nb	Hf	Ta	Th	Rb	Sr	Ba	Pb
U	1																	
Sc	0.162	1																
V	-0.16	-0.168	1															
Cr	0.226	0.37	0.029	1														
Co	-0.235	-0.053	-0.046	-0.848	1													
Cu	0.229	0.519	-0.136	0.916	-0.643	1												
Ga	0.139	-0.022	0.391	-0.334	0.101	-0.507	1											
Y	0.255	0.436	-0.255	0.465	-0.468	0.527	0.039	1										
Zr	0.886	0.292	-0.079	0.473	-0.511	0.391	0.236	0.319	1									
Ti	0.982	0.062	-0.121	0.149	-0.211	0.123	0.199	0.229	0.831	1								
Nb	0.478	0.435	0.211	-0.248	0.301	-0.177	0.641	0.288	0.41	0.472	1							
Hf	0.875	0.259	-0.119	0.499	-0.549	0.389	0.221	0.33	0.991	0.829	0.342	1						
Ta	-0.151	0.195	0.214	-0.434	0.746	-0.264	0.14	-0.222	-0.331	-0.16	0.499	-0.386	1					
Th	0.883	0.057	-0.176	0.459	-0.45	0.388	-0.136	0.109	0.829	0.873	0.089	0.848	-0.359	1				
Rb	0.21	0.622	-0.281	0.773	-0.465	0.903	-0.638	0.33	0.352	0.095	-0.185	0.338	-0.198	0.41	1			
Sr	0.694	-0.405	-0.165	-0.363	0.126	-0.426	0.309	-0.052	0.425	0.776	0.359	0.432	-0.021	0.552	-0.426	1		
Ba	0.689	-0.007	-0.029	-0.002	-0.005	-0.043	0.347	0.182	0.588	0.715	0.599	0.568	0.268	0.567	-0.06	0.706	1	
Pb	0.265	0.244	0.173	-0.339	0.18	-0.354	0.843	0.331	0.279	0.277	0.824	0.236	0.188	-0.152	-0.466	0.309	0.318	1

Table 7.6. Correlation matrix of LREEs with U and Th

	U	Th	La	Ce	Pr	Nd	Sm	Eu
U	1							
Th	0.883	1						
La	0.944	0.924	1					
Ce	0.946	0.895	0.989	1				
Pr	0.934	0.846	0.978	0.993	1			
Nd	0.894	0.736	0.916	0.954	0.979	1		
Sm	0.824	0.599	0.815	0.877	0.915	0.971	1	
Eu	0.634	0.305	0.55	0.636	0.675	0.763	0.877	1

Table 7.7 Correlation matrix of HREEs with U and Th

	U	Th	Gd	Tb	Dy	Ho	Er	Tm	Yb	Lu
U	1									
Th	0.883	1								
Gd	0.77	0.498	1							
Tb	0.594	0.37	0.805	1						
Dy	0.384	0.24	0.574	0.936	1					
Ho	0.29	0.175	0.447	0.882	0.976	1				
Er	0.248	0.199	0.341	0.814	0.949	0.974	1			
Tm	0.294	0.268	0.318	0.788	0.94	0.95	0.978	1		
Yb	0.305	0.31	0.23	0.703	0.87	0.902	0.948	0.974	1	
Lu	0.344	0.348	0.264	0.722	0.875	0.902	0.935	0.97	0.993	1